ALMA MATER STUDIORUM · UNIVERSITÀ DI BOLOGNA

SCHOOL OF
ENGINEERING AND ARCHITECTURE
- Forlí Campus -

Master's Degree in Aerospace Engineering
class LM20

GRADUATION THESIS:
in Experimental methods in aerodynamics

Wind Tunnel Analysis of an Automotive Wheel and Comparison with Numerical Simulations

Candidate :
Riccardo Barberini

Supervisor :
Prof. Gabriele Bellani

Academic Year 2018/2019

Contents

List of Figures

List of Tables

Abstract

The main purpose of this thesis is to find a relation between the results obtained with numerical simulations and the results coming from the experiments in the case of an automotive wheel. Before this study, it was investigated the phenomenon of the vortex shedding of a 2D cylinder. It was proven that the shedding frequency has a linear relation with the free stream velocity and this relation depends on the Strouhal number. The last stage of this acquistion campaign was to compare the calibration of the hot-wire anemometer with the Pitot probe and the calibration exploiting the vortex shedding frequency, obtaining very similar results.

The second step of this study was focused on the wake of three different type of wheels (sharp shoulders, 45 degrees shoulders and rounded shoulders) discovering that the sharp one generates a much larger wake than the other two. Also the Cd was evaluated, through the Trefftz plane method, obtaining a value of 0.98 for the rounded shoulders and 1.3 for 45-degrees one. The wake develpoment was very similar between the 45 degrees shoulders and rounded one. It was also studied the effect of some angles (camber and toe) on the rounded shoulders wheel, the camber (with an angle of -3.5°) produces an asymmetry of the wake, while the toe angle (with an angle of -0.5°) does not affect too much the results. The comparison with the CFD was made with the wheel without any angles of toe and camber[1]. Similar results were obtained in the wake shape and in the evaluation of the Strohual number. In particular the wake shape (visualized through the velocity contours) was compared with the solution of the RANS equations with Spalart-Allmaras turbulence model. Furthermore, the spectral analysis was compared with the Detatched-Eddy-Simulation. Both the S-A and the spectral analysis show a good match between numerical results and experimental ones.

Chapter 1

Introduction

Since the dawn of the motorsport, the aim of engineers was to build the fastest car possible. In order to do that two requirements must be fulfilled: reduce the drag and increase the downforce. The increasing of the downforce is useful in order to increase the velocity of the car during corners and turns, the reduction of the drag permits the car to reach the highest possible velocity in the straights. Before the installation of the wings, the cars were designed to have the lowest drag possible, they are known as cigar shape car. The reason why engineers adopted this shape was to minimize the form drag as low as possible, dealing only with skin friction. Obviously the performances in terms of cornering speed of those cars were miserable due to the absence of any wings that can increase the downforce, hence, increasing the adhesion force of the car to the ground. With the arrival of the wings F1 cars were capable to decrease a lot the time lap of the circuit. Even if more than 1000 grand-prix are passed, there is still one common point: the wheels. The wheels have changed size due to regulations and safety reasons but still they are uncovered and they are the part of the car that mostly affects the drag, almost 40% of the total drag [2]. The study of the wake generated by a wheel is paramount for understand the physics and try to invent ways in order to reduce the drag of the total car, knowing how the wheel interacts with the car. This study can be faced in two different ways: numerically or experimentally. In this case it was chosen the experimental point of view and in particular the task was to compare the results obtained with the ones coming from the CFD study, already existing. The determination of a relation between numerical and experimental results is really important for engineers, it can permit ,in fact, to validate several simulations technique and understand which one is better to use in different situations.

Before focusing on this problem an intermediate step was performed: the study of the 2D cylinder (with a diameter of 80mm) in a cross-flow through the hot wire anemometer. It was obtaiend the mean velocity wake profile, it was computed the spectral analysis and the Strouhal number. Succesively it has gone from the 2D world to the 3D with 3 different wheels (with different type of shoulders: sharp, 45°, and rounded) at different distances and different geometrical variables (camber and toe angle in the case of rounded shoulder). Finally, the comparison with the CFD results were performed. In order to better simulate the reality the three wheels were put near the ground.

In the following chapters it will be illustrated the necessary aerodynamic theory in order to better comprehend this study: a brief introduction in the aerodynamic world and a specific focus on the phenomenon of vortex shedding and the behaviour of the wake of a bluff body. After this section an explanation of the methods used to study the data obtain from the experiments is explained. At the end there are presents the results obtained in both 2D and 3D cases and the conclusions.

Chapter 2

Theoretical background

2.1 The equations

The aerodynamics field is governed by the Navier-Stokes equations. It is a set of three equations that describes how a generic fluid interacts with a body immersed in it. The three equations are: conservation of mass, momentum balance and balance of the energy. The latter one can be neglected if it is assumed that the viscosity is constant (condition that hold true for most of the automotive cases). The conservation of mass is a scalar equation while the momentum balance is a vector equation of three components: x,y,z. Considering that the unknowns are the pressure (p) and the three component of the velocity vector (u,v,w) the problem can be considered mathematically closed, 4 unknowns in 4 equations. Before starting with the equations one hypothesis have to be made: the aerodynamic field deals with the continuous world, this means deal with average quantities inside a small volume. This volume is called fluid particle and must be large enough in order to contain a good amount of fluid molecules that can permit to extract a reliable average value for all the quantities. Let's have a look now on the equations.

The mass conservation has this form:

$$\frac{\partial u}{\partial x} + \frac{\partial v}{\partial y} + \frac{\partial w}{\partial z} = 0 \tag{2.1}$$

This means that the variation of the velocity in the three directions must be zero.

The momentum balance is:

$$\frac{\partial \vec{V}}{\partial t} + \vec{V} \cdot \nabla \vec{V} = \vec{f} - \frac{1}{\rho}\nabla p + \nu \nabla^2 V \tag{2.2}$$

This is written in the vectorial form, this must be split in its three components. The left hand side of the equation is the sum of the contribution of unsteady term and convective term while the right hand side represents the force per unit mass. It is composed of gravity term (that is the volume force), pressure stresses and viscous stresses that together form the surface forces. The viscous stresses are divided in their two components: the one normal to the surface particle and the one that is tangential. The stress tensor is defined as:

$$\tau_{ij} = \mu\Big(\frac{\partial u_i}{\partial x_k} + \frac{\partial u_k}{\partial x_i}\Big) \tag{2.3}$$

It can be seen that there is a relation between the components of the velocity vector and the stress tensor, this will

be recalled when it will be introduced the procedure to solve the aerodynamics problem. Now it must be introduced another variable, the vorticity. The vorticity is defined as follows:

$$\omega = curl\vec{V} \tag{2.4}$$

Once the velocity is known it is known also the vorticity and vice versa. Making the momentum balance of the vorticity :

$$\frac{\partial\vec{V}}{\partial t} + \omega xV = -\nabla\big(\frac{p}{\rho} + \frac{V^2}{2} + \Omega\big) - vcurl\omega \tag{2.5}$$

Form here, making the hypothesis of irrotational flow it is lost the viscous term (the curl of omega is equal to 0) and by adding the presence of a steady flow it will obtained the Bernoulli equation:

$$\frac{p}{\rho} + \frac{V^2}{2} + \Omega = constant \tag{2.6}$$

The condition of irrotationality implies also:

$$\vec{V} = \nabla\Phi \tag{2.7}$$

If this expression is put in the conservation of mass it is obtained:

$$\nabla^2\Phi = 0 \tag{2.8}$$

This formula, however, holds true only for irrotational flow, but due to no slip condition at the boundary of a generic body it is impossible to have irrotational flow. In fact on the surface of the body in exam it is possible to put two different boundary conditions: no slip boundary condition (called also Dirchlet from a mathematical point of view) or no penetration condition (called also Neumann boundary condition). While the first is more restrictive, in fact requires that the relative velocity to the wall of a fluid particle is equal to zero, the latter one is more permissive: only the vertical component of the velocity is set to zero on the boundary, meaning that the flow must not penetrate the surface of the body. Having irrotational flow means to adopt a Neumann boundary condition, thus no vorticity can be generated. [5]

2.2 The boundary layer

So why it is necessary having two type of boundary conditions? If it is impossible to have an irrotational flow it seems that the no penetration condition is useless. The answer of this question is given by Prandtl. Prandtl found that on the surface of the body it exists a region called boundary layer in which the effect of the viscosity it is not negligible, furthermore it discovered that the velocity of a fluid particle goes from zero to the one of the free stream at the edge of the boundary (where the flow can be considered irrotational) and there is no pressure variation along the thickness of the boundary layer. This discovery is a masterpiece for aerodynamics, in fact knowing the pressure on the wall of a body means also know the pressure on the edge of the boundary layer. To solve a generic aerodynamic problem an iterative process is needed: the first step implies to put the thickness of the boundary layer equal to zero (this does not mean that does not exists at the first iteration). The no penetration condition is now used in order to solve the problem and know the pressure distribution on the boundary, once the pressure distribution is known it is possible to know the tangential stresses and the thickness of the boundary. The thickness will be the input of the second iteration and so on.

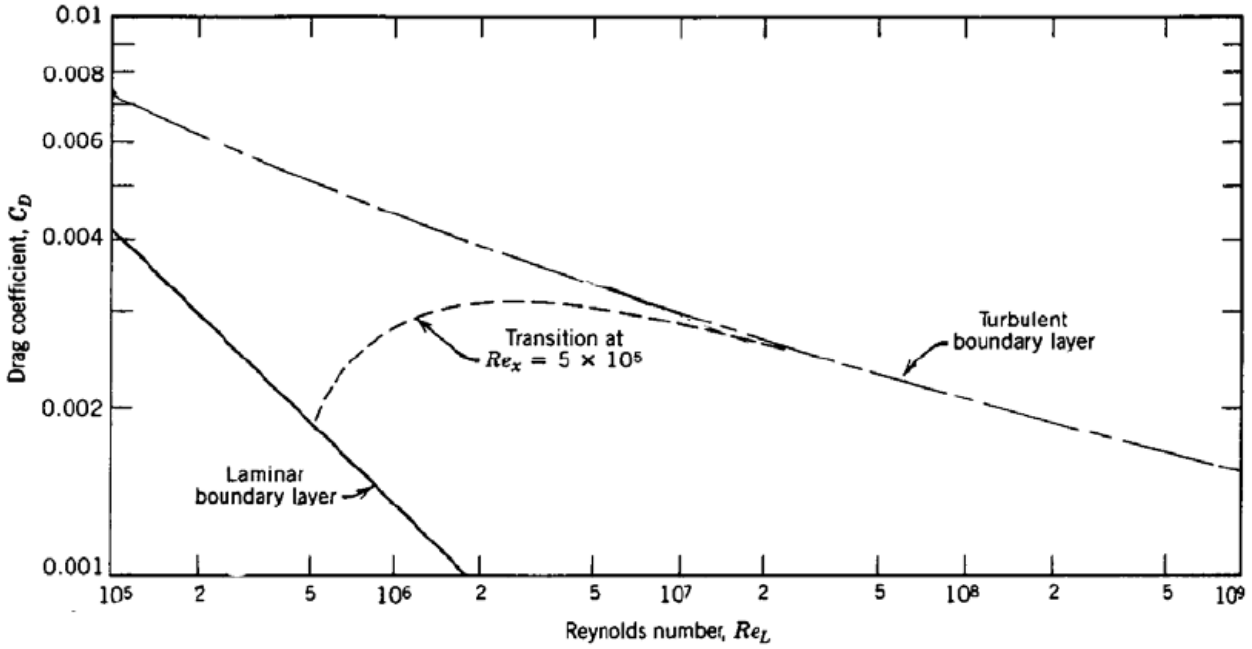

Figure 2.1: *Hermann Schlichting [3]Cd-Re graph. It can be seen how the presence of a laminar boundary layer leads to a lower drag coefficient (in this case it is considered only the skin friction not the effect of 3D)*

The procedure stops when the value of the pressure in two adjacent iteration is almost equal. In order to obtain the forces acting on the body it must be integrate the value of the tangential stresses and the pressure distribution. The boundary layer is born when the fluid particles hit the surface of the body and its behaviour along the longitudinal direction of the body depends mainly from the pressure gradient that the boundary layer encounters: in presence of negative pressure gradient the boundary layer accelerate and becomes thinner penetrating more and remaining more attached to the body remaining laminar. This condition is the one that engineers want in order to reduce the drag, later it is explained why. On the other hand in presence of adverse pressure gradient the boundary layer does not have enough energy to penetrate and it separates. This condition is reached when the velocity profile of the boundary layer has an inflexional point. After this point the flow is no more attached to the body, this region is called wake. It is obvious to understand that the iterative procedure explained before is valid only in the case of a boundary layer attached to the surface. The reason why it is preferable having a laminar boundary layer rather than a turbulent one is given by the drag that born in the two different cases as shown in the following figure. There is a linear relation between the skin drag coefficient and the Reynlods number and the slope of the relation depends on the flow regime: the slope in the case of a laminar flow is -2/3 while for a turbulent is -5/3.

2.3 The vortex shedding

The bodies in the aerodynamic world are divided in two families: aerodynamic bodies, bluff bodies. The aerodynamic bodies are the one that have the boundary layer attached to their surface for most of the length of the body and have a small base (the base is the height of the wake). The bluff bodies, on the contrary, have a larger base due to a more anticipated detachment of the boundary layer. Another feature that can permits to identify if a body is bluff or aerodynamic is the ratio between lift and drag, called aerodynamic efficiency. Usually aerodynamic bodies have larger

efficiency than the bluff bodies, it must be said that aerodynamic bodies can become bluff bodies once they have a wrong attitude with respect to the flow. For instance, a wing with 45 degrees of angle of attack can be considered a bluff body. Considering that this study is oriented on the wake of a wheel (one of the most famous bluff bodies) let's put aside the aerodynamic bodies and let's focus on the bluff bodies.

The family of the bluff bodies can be divided in two groups: free separation and fixed separation bodies. As their name suggests, the free separation bodies are those ones in which the boundary layer separates accordingly to the pressure gradient (as explained before). The fix separation ones separate in a given point, without the dependence on the external factor. In order to give a better understanding, an example of free separation body is a cylinder, an example of a fix separation body is a squared prism. Now it will be explained more accurately this concept. Starting from the circular cylinder, the boundary layer separates in different positions depending on the flow regime. Three main regions can be identified: subcritical, critical and supercritical.

The subcritical region is for $Re < 5 \cdot 10^5$. In this region the flow is still laminar, even if the flow has low intensity the drag produced is higher, in order to understand this, three main aspects must be taken into account. The first is the separation point. In this case is placed at almost 84°, the flow it is not able to penetrate inside the pressure gradient given by the geometry. It can be raised the question about why the separation point is not exactly at 90°. This is due to the subsonic condition, the information of the adverse pressure gradient propagates backwards and for this reason the separation point is anticipated by 5/6°. The separation point leads to confer the wake to have a certain base, in this case the length of the base is large and implicates having a large drag. The second aspect is given by the formation of the vortex, being the flux laminar the vortex created at the separation point have an higher intensity because they are more compact this means bring more vorticity in the wake, increasing the drag force. The last point is the relative influence that the upper and lower vortices have: being the wake wide the annihilation given by the vortex with opposite value of vorticity will be low.

In the supercritical region, happens exactly the opposite, this justify a lower value of the drag coefficient. The boundary layer is now turbulent, thus it can go deeper into the pressure gradient, separating almost at 120°. This separation point leads to have a narrower base, so a smaller wake. Furthermore at the separation point, when the vortex is rolled up, the vortex will have a lower intensity due to the minor compactness of the vorticity, thus minor vorticity is released in the wake. The narrower wake implicates that the vortices annihilate each other more than in the previous case. All these three aspects bring having a lower Cd in the supercritical regime. The most interesting region is the critical one. Here it exists a plateau where the drag is reaches the minimum value. The explanation of the behaviour is to a attribute to the separation line. It must be imagined to see the cylinder in 3D, in the case of subcritical and supercritical region the separation point was fixed in a certain point, this brings in 3D to have a straight separation line. In the case of the critical region the separation line is not straight, this is due to the phenomenon of transition. The transition of the boundary layer from laminar to turbulent is mostly affected to external disturbances (as surface roughness). In the transition it is possible to see at different length of the cylinder separation point at different locations. Not having a straight separation line means the lack of vortex produced. In fact, for the Naumann condition, in order to a vortex be crated it is necessary to have a separation line that coincides with a generatrix of the body. The lack of vortex is the reason why it exists that plateau. There is a relation between the surface roughness of a cylinder and the position of the critical region. In particular, increasing the roughness of the surface the plateau region is anticipated. With the exception of the critical regime, when the flow encounters a cylinder there is the formation of vortices. The first who discovered it was Von Karman, he saw an alternating creation of vortex in the upper and lower part of the cylinder. He was able to derive the drag produced knowing the intensity of the vortices and the distance between those [6].

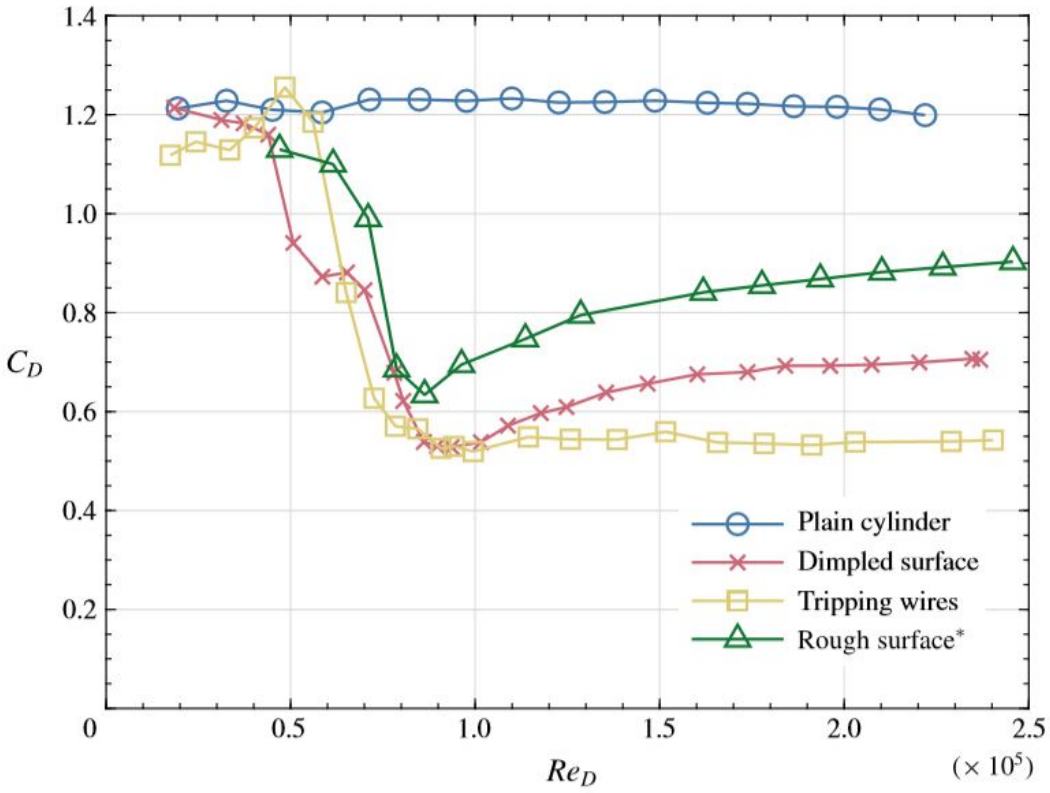

Figure 2.2: *Ben L. Clapperton and Peter W. Bearman [4]. Dependence of the drag coefficient to the Reynlods number. The postion of the plateau depends on the surface roughness of the cylinder.*

$$F_D = \rho\Gamma\frac{h}{l}\left(V - V_v\right) + \rho\frac{\Gamma^2}{2\pi l} \tag{2.9}$$

With l that is the longitudinal distance between two vortices and h is the spanwise distance. Γ is vortex intensity and and Vv is the translation velocity of the vortices with respect to the flow that can be obtained from:

$$V_v = \frac{\Gamma}{2l}\tanh\frac{\pi h}{l} \tag{2.10}$$

These two relations even if they are useful are difficult to use, in fact it is very difficult knows a priori the distance between the two vortices and their intensity given a certain body. The phenomenon of the formation of the vortex in a bluff body is known as vortex shedding and even if a lot of research has been made on this subject, nowadays is still one of the most interesting aerodynamic problem to investigate. The formation of the vortex shedding starts from a value of the Reynlods number equal to 47 almost. For a range between 0 and 47 there exists a stable configuration in which is present a recirculation region which increases its dimension for an increasing Reynlods number. This configuration is stable up to the point in which two alternating vortices starts to detach from the body for a given frequency. An interesting study on the stability analysis of the wake of the bluff body was made in the last century. Before talking about the results obtained it is useful to introduce some definition regarding the stability analysis. A velocity profile is said to be locally absolutely unstable if a localized disturbance is spread both downstream and upstream. If the disturbance is swept away only downstream we are talking about locally convectively unstable velocity profile. In the

case of the vortex shedding, in wake regions near the body the velocity profile is absolutely unstable while in regions far away the profile becomes convectively unstable. Those conditions can be changed in stable if it is introduced in the wake the effect either of suction or blowing. For instance it was proved that over a certain amount of suction the wake becomes stable. It was discovered also that the lack of the vortex shedding in addition to already mentioned not straight separation line, can be obtained for different values of the velocity between upper and lower part of the cylinder.

Previously, talking about subcritical and supercritical region, it was sentenced that every time a vortex detaches from the body a finite amount of vorticity is introduced in the wake. In order to evaluate this amount it was found that the instantaneous flux of vorticity is:

$$\frac{\partial \Gamma}{\partial t} = \frac{1}{2}\left(V_s^2 - V_b^2\right) \tag{2.11}$$

With V_s that is the velocity out of the boundary layer in the separation point and V_b the velocity in the same point of the base. In order to evaluate the amount of vorticity in a certain period $T = 1/fs$ (fs is the shedding frequency) this relation must be integrated in time in the same period. Comparing the results of the measured vorticity evaluated

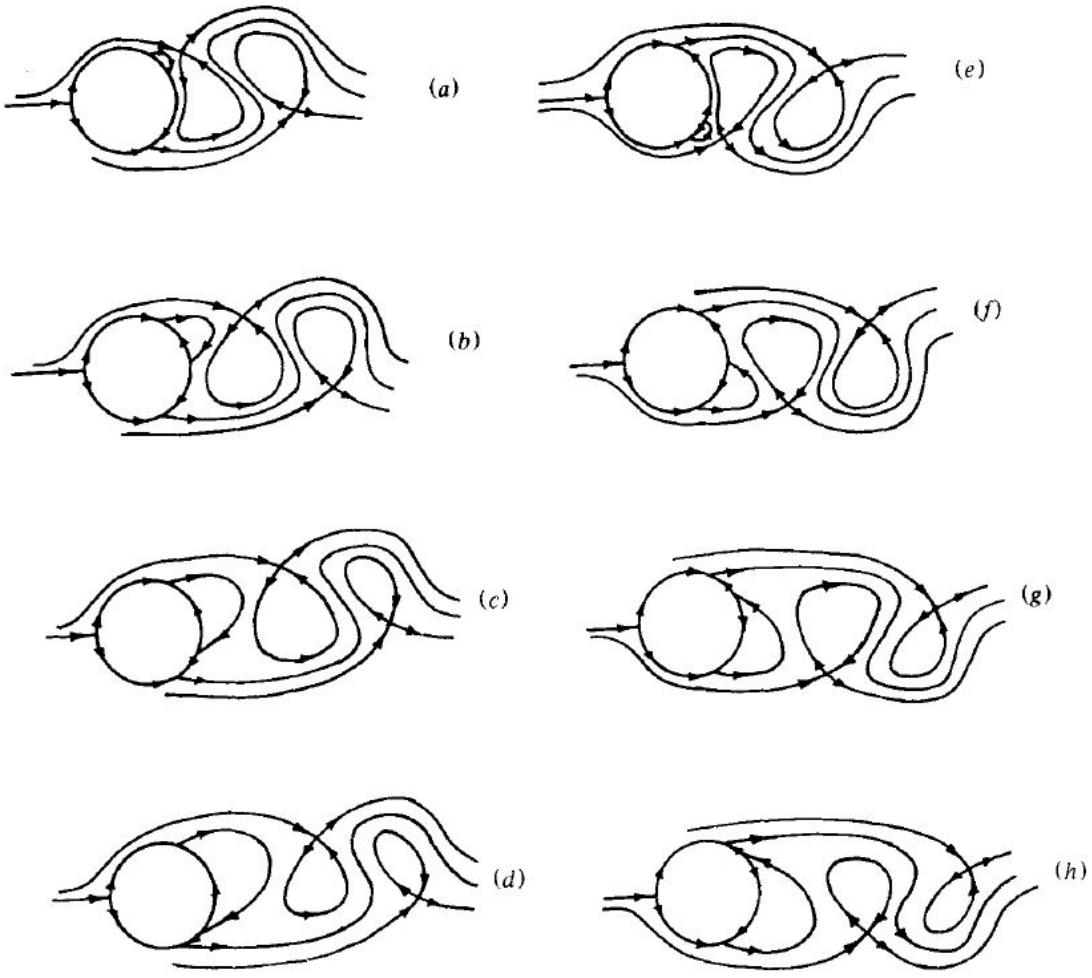

Figure 2.3: *A.E.Perry, M.S.Chong and T.T.Lim[7]. Behaviour of the flow for different ranges of Reynlods number. The stable condition holds until Re 40 then the vortex shedding occurs. The vortex shedding then disappears when the Reynolds number lies in the critical region.)*

downstream, it was founded that only the 40/60% of the vorticity survives the formation process. There are different reasons why this happen; it can be due to the presence of the oscillating component of the velocity which brings an underestimation of the vorticity introduced from the base. An experiment conducted by Cantwell and Coles in 1983 stated that "turbulent mixing by convection at inviscid scales, rather than turbulent diffusion at viscous scales, is probably a sufficient mechanism to account for much of the cancellation of mean vorticity in the base region". Perry in 1982 proposed a simplified model of a shedding cycle, proposed in the next figure [7]

. The left column shows the evolution in time of the upper vortex while the right one the evolution of the lower vortex. The white closed regions are called saddles and contain one vortex each. The saddles are divided by a continued line called alleyways. It can be said that the shedding of a vortex occurs when one saddle already formed reaches the separation saddle opposite to the one it stems from.

The frequency of the vortex shedding has a linear relationship with the free stream velocity in particular:

$$f_s = \frac{St \cdot U}{D} \tag{2.12}$$

Where U is the free stream velocity, D is the diameter of the cylinder in exam and St is the Strouhal number. The Strouhal number is a variable which value is between 0.18 and 0.22. At the end of the previous century it was found a relation between the Strouhal number and the Raynolds number. This relation changes depending on the range of interest, figure 5 illustrates this relationship. For an increasing of the Reynolds number there is a linear increment of the Strouhal number up to a certain condition in which the relation changes slope and tents to decrease.

It can be seen that the strouhal number reaches its maximum value for Reynolds number almost equal to 1300, then entering in the subcritical regime it decreases its value.[8]

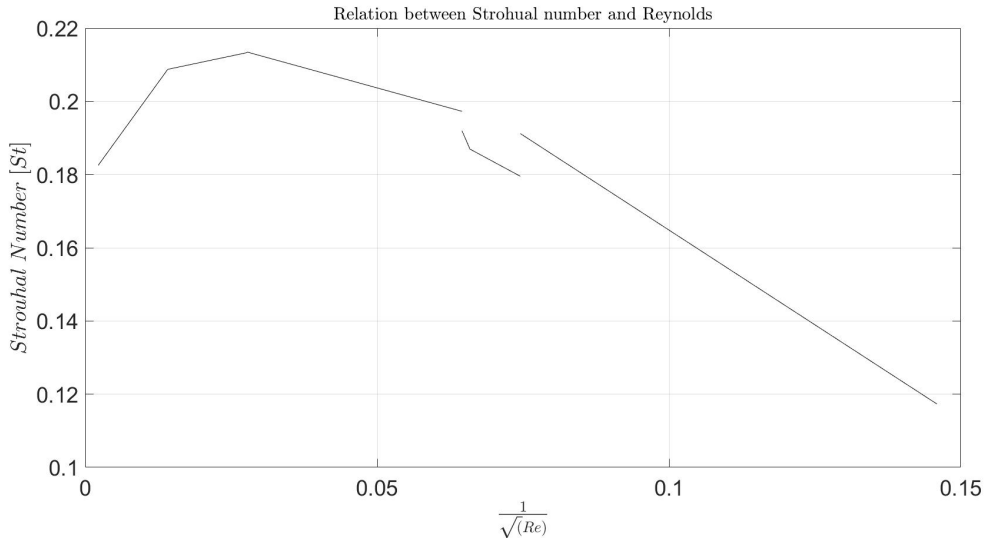

Figure 2.4: *Uwe Fey, Michael König, and Helmut Eckelmann 1998[8]. Strouhal Reynolds relationship. On the x axis the Reynlods number is represented as* $\frac{1}{\sqrt{Re}}$ *so higher value of the Reynlods are at the left of the graph. The maximum value is reached for a Reynolds near to 1300)*

Reynolds range	St	M
47<Re<180	0.2684	-1.0356
180<Re<230	0.2437	-0.8607
230<Re<240	0.4291	-3.6735
240<Re<360	Depends on the B.C.	Depends on the B.C
360<Re<1300	0.2257	-0.4402
1300<Re<5000	0.2040	0.3364
$500 < Re < 2 \cdot 10^5$	0.1776	2.2023

Table 2.1: *Resuming table of different behaviour of Strouhal number depending on the Reynolds number range.*

Since the last step of this study is the evaluation of the wake of an isolated wheel near the ground, it is interesting to see the intermediate step between the 2D cylinder and the wheel near the ground: a 2D cylinder near the ground.

It was found that the Strouhal number was independent from the ratio G/D for G/D>0.3, under this value the vortex shedding is suppressed. By the reading of the pressure measurements, for low values of gap-to-diameter ratio the front stagnation point was rotated towards the plane wall giving a forcing lift to the cylinder moving away it from the wall. When the cylinder was put attached to the wall the upstream and downstream separation regions were attached to the cylinder and no regular vortex shedding was observed. For gap ratios between 0.5 and 0.75 an alternating vortex shedding was found but with a lower strohual number. It was also seen that the flow detaches form the ground downstream of the cylinder and the frequency of this separation is coupled with the vortex shedding of the cylinder. For gap ratio between 0.25 and 0.375 it was seen a separation region upstream the cylinder and this region decreases as the gap ratio increases. The shear layer shed from the outer surface shed in a periodic manner but this phenomenon can not be seen as the vortex shedding, while the inner does not shed unlike the outer layer. [9]

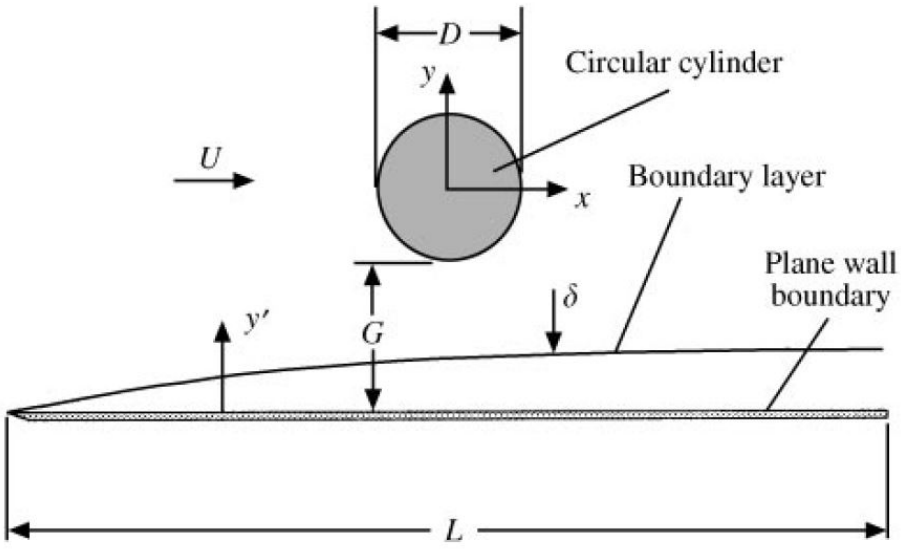

Figure 2.5: *S.J. Price, D.Sumner.[9] Representation of the experiment conducted by Price in 2002 evaluating the behaviour of the vortex shedding at different height form the wall*

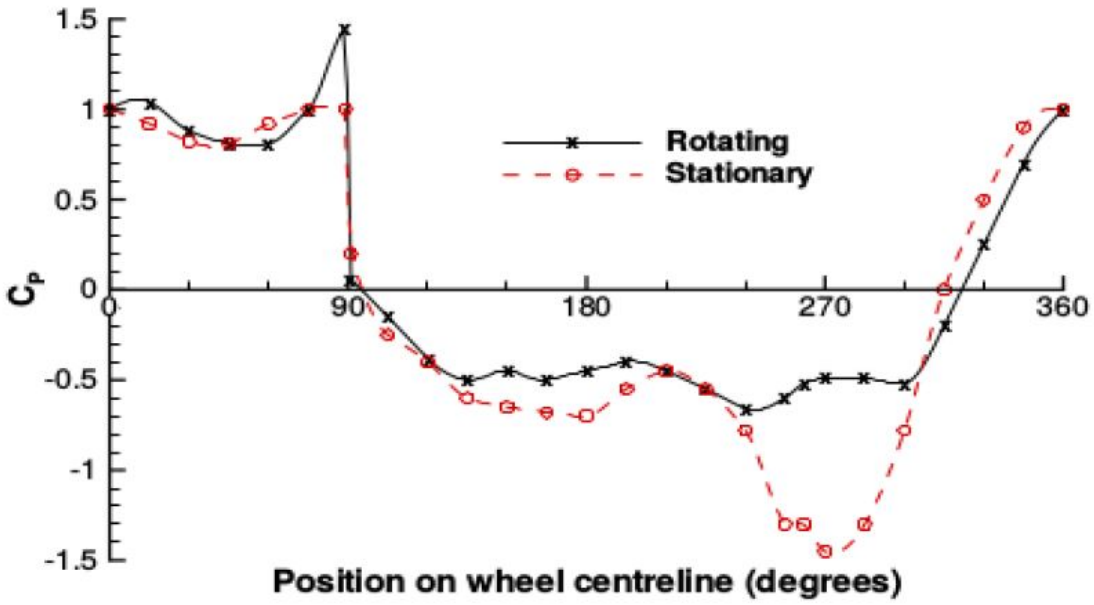

Figure 2.6: *Fackrell [10] Differences between Cp value of stationary wheel and rotating. It is interesting to see that the lower peaks are obtained for the stationary case while the higher one for the rotating case.*

2.4 Aerodynamic of a wheel

Due to technology limitations it was not possible to conduct experiment with a rotating wheel inside the wheel tunnel, all the results obtained will refer to a stationary wheel in contact with the ground. Considering that most of the literature deals with rotating wheel, even if the results will be different it is interesting, however, to see how the flow behaves around a 3D bluff body.

An interesting comparison between the stationary and rotating wheel can be done looking at the pressure distribution around the wheel. It can be seen from the figure that higher positive peaks are reached by the rotating wheel while the negative peaks are obtained for the stationary. For the stationary case the flow is capable to be more attached to the surface, in the rotating case, instead, the flow is subjected to an high acceleration and it is not able to follow the curvature, this leads to a fully turbulent separation. In particular Fackrell suggested that while the flow in the stationary case remains attached until 120° (as in 2D condition) in the case of rotating the separation point moves forward of 70°. The reason why the Cp reaches values higher than 1 is due to the squeezing action of the air by the ground. Focusing on the wake structure of the stationary case study have shown that the wake is smaller rather than the rotating case and has stronger lower vortices. This happen because the flow has to go down to the rear face before rolling up, for rotating one vortices are formed by a lower recirculation area in rear region. In the following figure it can be seen the bulges near to the ground, they showed the presence of a vortex shed from either side of the front wheel, where local vorticity created in the flow by the movement around the base of the wheel had pooled and formed a stable vortex core.[10] This features are valid for a wheel with in a neutral camber position. The camber angle is the angle between the vertical axis of the wheel and the vertical plane. The camber angle can be positive, neutral or negative. The positive camber is obtained inclining the wheel towards the outside while a negative camber is obtained inclining the wheel towards the inside of the car. The positive camber is mostly used in the off road applications while the negative one is installed in race cars. The negative camber is useful in the corners, in particular it improves the cornering grip because the

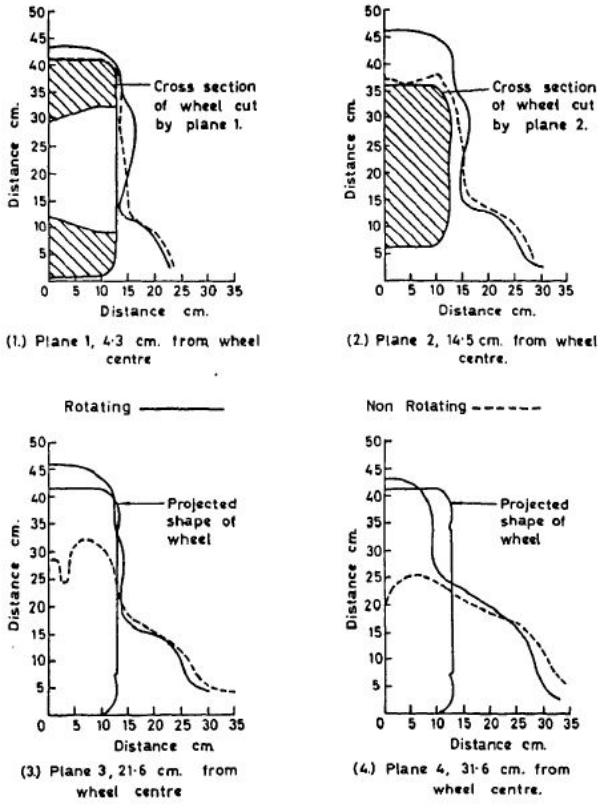

Figure 2.7: *Fackrell [10]. Comparison of wake dimension between rotating and stationary wheel at different distance form the wheel istelf.*

outer wheel generates a greater lateral force on the entry to a corner. The drawback is the behaviour of the wheel in the straights, in fact during the straights both wheels will suffer an higher consumption on the inner shoulders of both wheels, this over consumption of the wheel can bring the wheel to generate blistering. A lot of research has been been made in order to understand how the wake is affected by the camber angle. An interesting results was derived by Robin Knowles, Alistair Saddington and Kevin Knowles who, through the PIV measurements found the creation of a larger vortex in the portion of the wheel that is more in contact with the ground.[11] The drag is influenced as well in the cambered condition, due to the asymmetry of the wake. In particular the ratio between the drag in the parallel condtion and with the camber angle is equal to 0.8. The toe angle is defined as the angle between the axis of the wheel and the direction of the velocity vector. As well as the camber angle, the toe can be negative, neutral or positive. The positive toe is obtained by directing the wheel to the inside of the car (from a top view) while a negative toe is reached when the wheel point outside the car. The toe angle is used in order to correct the car behaviour during corners, avoiding understeer or oversteer. As it happens for the camber, the performance of the car during straight is decreased using a toe angle due to less contact patch area rather than a neutral condition.

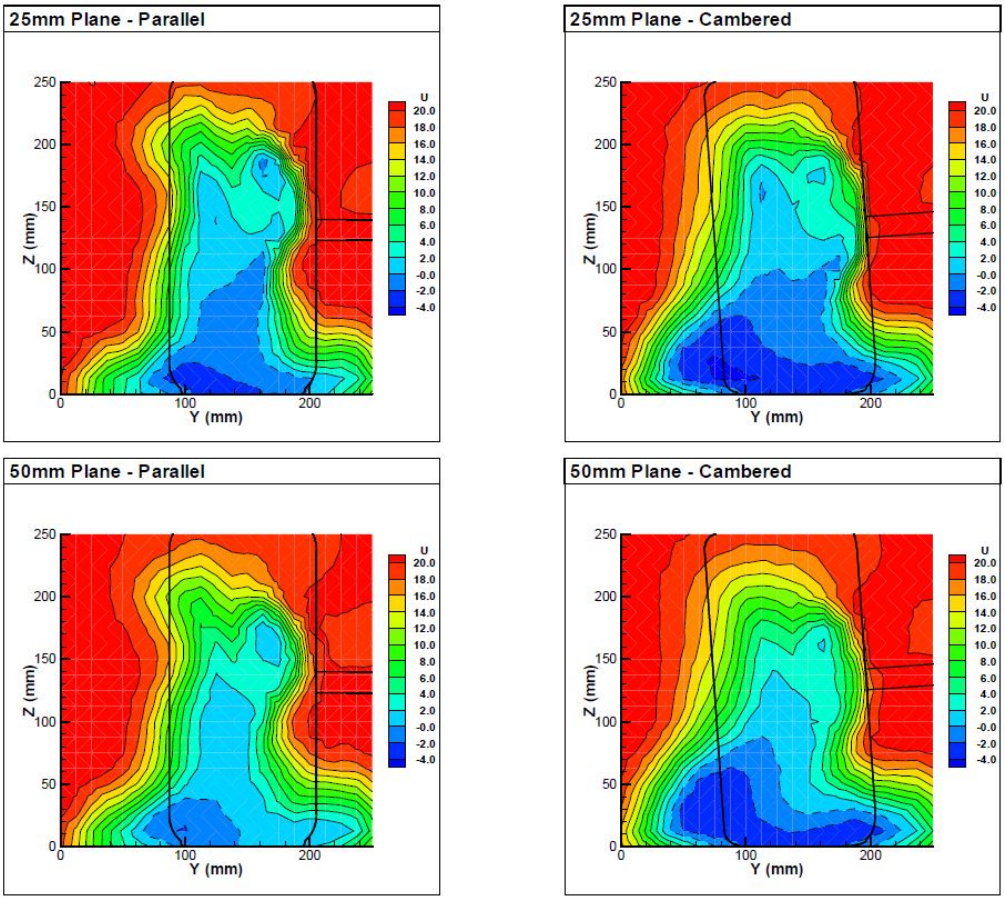

Figure 2.8: *Robin Knowles, Alistair Saddington [11]Difference between parallel and cambered wheels. The presence of a bigger vortex is felt in the cambered configuration, leading to have a greater resistance.*

2.5 Matematical methods

To understand the physics of the problem it is necessary to adopt different mathematical methods in order to get the right information. In the following sections there will be illustrated the definition and the meaning of the statistical moments, the Fourier transform and the Hamming windowing . The statistical moments are useful when using mean values, the other methods are used for comprehend the shedding frequency.

2.5.1 Statistical moments

The most used statistical moments are: mean, standard deviation, skewness and the kurtosis. Each of these moments carry an information of the signal. The easiest one to comprehend is the mean. The mean is the most frequent value in a set of data. The standard deviation reveals how much the data are spread out from the mean value. An high value of standard deviation means a big uncertainty on the data (mostly due to the presence of noise in the signal), it can be seen as a confidence interval. The skewness reveals if the data are asymmetric with respect the mean. A positive skewness is an indication of a distribution shifted to the left while a negative skewness implies having a distribution shifted to the right. A null skewness is a symmetric distribution. The last moment is the kurtosis, the kurtosis is an index of the importance of the tails of the distribution curve. For a kurtosis less than 3 means having fewer and less extreme outliers

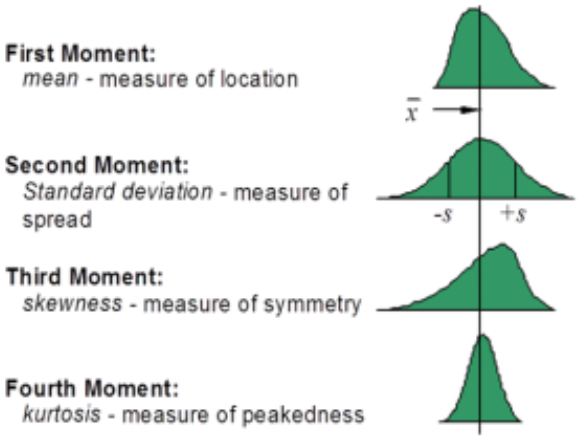

Figure 2.9: *Representation of the most famous statistical moments.*

than the normal distribution, in this case the distribution is said to be "platykurtic". In the opposite case the distribution is called "leptokurtic".

These mathematical tools are very useful for the wake evaluation of the 2D cylinder. It will be shown in the results that the minimum value of skewness is the indicator of the edge of the wake, while the highest standard deviation is and indicator on the maximum gradient reached in the wake profile. From a mathematical point of view the statistical moments can be defined as:

$$M_r = \frac{1}{N}\sum_{i=1}^{N}\left(X_i - \bar{X}\right)^r \tag{2.13}$$

With N that is the number of data and r is the moment in exam, reminding that the mean is the first moment, the second moment is the standard deviation, then the skewness and finally the kurtosis.

2.5.2 The Fourier transform

The Fourier transform it is used in this study in order to get the power spectrum of both the cylinder and the 3D wheel. Other operation associated with FFT are: the convolution of two time series to perform digital filtering and the correlation of two time series. In particular it was used a specific Fourier transform, called Fourier Fast Transform (FFT). The FFT takes the signal in the time domain and it converts it to the frequency domain, in this way it is possible to find the characteristic frequency of the signal. This algorithm reduces the computational cost maintaining similar results. Working with sampled data means working with a finite number of element, thus the discrete Fourier transform (DFT) must be used. The FFT is an efficient method of solving DFT. The DFT can be written in this way:

$$X(j) = \frac{1}{N}\sum_{k=0}^{N-1} x(x)e^{-\frac{i2\pi jk}{N}} \tag{2.14}$$

$$x(k) = \sum_{j=0}^{N-1} X(j)e^{\frac{i2\pi jk}{N}} \tag{2.15}$$

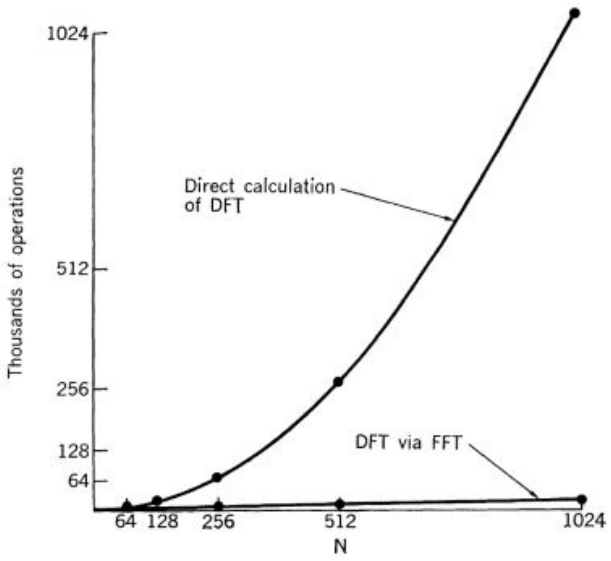

Figure 2.10: *G. D. Bergland [12]Computational cost comparison between direct calculation of DFT and calculation of DFT using FFT. In the x-axis is represented the number of elements inside the Fourier transform, in the y-axis the number of operations required.*

The proof of the previous statement regarding the computational cost of the FFT is given by the following figure. In particular the gap between DFT with FFT and DFT with direct calculation is very relevant at high values of N (number of elements inside the Fourier transform). For instance, for N=1024 there is a computational reduction of more than 200 to 1.

Some problems can be faced during the using of the FFT, the drawbacks that can afflict this study are: the leakages and the aliasing.[12] The leakages born with sampled signal, in particular when the signal to be studied is multiplied for a rectangular data window. Multiplying the signal for the data window is similar to perform a convolution in the frequency domain. The results are several spurious peaks called sidelobes and in addition the function it is not localized on the frequency axis.

It is easy to understand that the aim is to reduce at maximum the presence of the sidlobes, this can be done adopting a different type of data window. One of the most used is the Welch windowing which will be illustrated in the following section. The second problem that can rise is the aliasing. The aliasing phenomenon occurs when the sampling frequency is too low with respect the frequency of the signal to be sampled. The results is a signal sampled completely different from the real one. In order to avoid this phenomenon it is necessary to sample the signal with at least twice the frequency of the signal to be sampled. This is given by the Nyquist criterion.

Where is the difference between DFT and FFT? The difference lays in the number of computation. Taking the expression of the Fourier transform written before and write it in a matrix form (for N=4) it is obtained:

$$\begin{bmatrix} X(0) \\ X(1) \\ X(2) \\ X(3) \end{bmatrix} = \begin{bmatrix} W^0 & \dots & W^0 \\ \vdots & \ddots & \vdots \\ W^0 & \dots & W^9 \end{bmatrix} \begin{bmatrix} x(0) \\ x(1) \\ x(2) \\ x(3) \end{bmatrix} \tag{2.16}$$

In general to be solved the previous equation requires N^2 complex multiplication and addition, the FFT reduces this

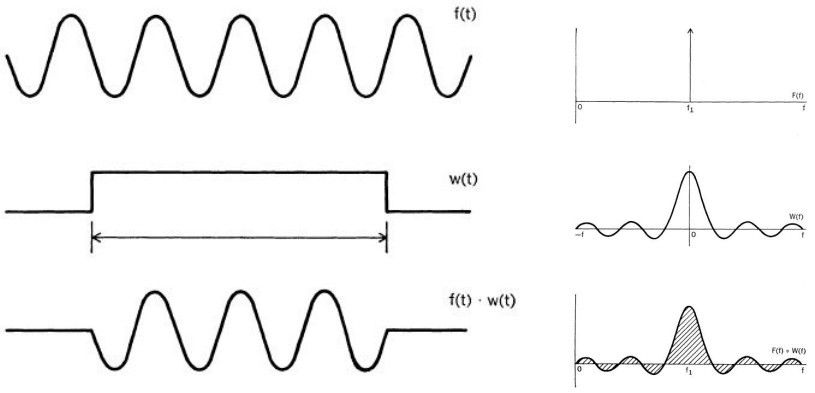

Figure 2.11: *G. D. Bergland[12] Example of how leakage effect occurs. The moltiplication of the sampled signal with the rectangular data window is the cause of this effect.*

operation, reducing the computational cost.

2.5.3 The Welch's method

This method it is implemented in order to reduce the sidelobes present in the power spectrum using the FFT and decreasing the amount of noise present in the signal in exam. This process consists in creating a certain number of windows of the same length, overlap them by a distance equal to half the length of the window, evaluate the FFT of each window and obtaining the mean value from the all results. In this case, the function that represents the window it is not a rectangular function but it is rounded at the boundaries (Hamming window). The function that in exam is given by:

$$W(j) = 1 - \left(\frac{j - \frac{L-1}{2}}{\frac{L+1}{2}} \right)^2 \tag{2.17}$$

Where j that goes from 0 to L-1 (L is the length of the signal segment). This window is put in the Fourier transform:

$$A_k = \frac{1}{L} \sum_{j=0}^{L-1} X_k(j) W(j) e^{-\frac{2kijn}{L}} \tag{2.18}$$

Where X_k is defined as:

$$X_k(j) = X\big(j + (K-1)D\big) \tag{2.19}$$

D is the value of how much the segments are overlapped each other and K is the number of segments. The results obtained from the Fourier transform are then insert in:

$$I_k = \frac{L}{U} |A_k|^2 \tag{2.20}$$

Where U is:

$$U = \frac{1}{L} \sum_{j=0}^{L-1} W(k)^2 \tag{2.21}$$

And finally:

$$P = \frac{1}{L}\sum_{k=1}^{L} I_k \tag{2.22}$$

The previous expression of W(j) is the one adopted for this study, it has the shape $1 - t^2$ and its shape is very similar to Hamming or cosine arch spectral window. The other possible shape could be:

$$W\left(j\right) = 1 - \left|\frac{j - \frac{L-1}{2}}{\frac{L+1}{2}}\right|^2 \tag{2.23}$$

This type of shape gives the Parzen spectral window.[13]

Chapter 3

Tools and facilities

To make possible the success of the experiments several tools are required. The most important is the wind tunnel facility, then the hot-wire anemometer necessary to measure the speed of the flow, the Pitot probe, used to calibrate the anemometer, and the data acquisition. Each of these tools has its role in the experiment, in this chapter will be illustrated the importance of them and how they work.

3.1 The wind tunnel

The wind tunnels can be classified in two families: low speed and high speed. The low speed work in subsonic condition while the high speed work in transonic and supersonic condition. Another distinction between the wind tunnel can be the type of the loop: open loop or closed loop. The open loop, as the one used for these experiments, are simpler to build but they are influenced by external conditions. Usually the open loop configuration is composed by: effuser, test section, diffuser and the fan driven by the motor. The effuser has the duty to accelerate the air prior the test section avoiding any separation of the flow near the walls and stretching the turbulent fluctuations. The test section is the place where the body that must be studied has to be installed. The test section must be accessible in order to install easily sensor and the body to study and one wall is made by glass or plexiglass in order to be able to watch inside the test section. The diffuser is the most delicate part of the wind tunnel, here the flow reduces its speed in order to have a pressure recovery. In this section the flow has an high probability to separate because of the increasing section, thus the flow feels an adverse pressure gradient. Considering that the wind tunnel works in subsonic condition any detachment of the flow in the diffuser is felt in the test section producing results different from the expected ones. The length of the diffuser determines the encumbrance of the overall wind tunnel. In order to avoid separation, the opening angle of the diffuser must be the lowest possible but this will bring the diffuser to have a longer length, thus increasing the encumbrance. There is an optimum angle that can be achieved avoiding the separation of the flow and this is almost equal to 3°. Another problem faced in the diffuser is the polygonal section due to the test section. If the diffuser had a polygonal cross section then there would be the development of corner vortices, for this reason there is a changing in the shape of the cross section of the diffuser from polygonal to circular. After the diffuser the motor with the fan are installed, this configuration is called suction because the air is sucked from the effuse to the fan. Another type of open loop wind tunnel is the blower type. In this case the motor is placed in front of the model, then a settling chamber is placed where the flow is relaxed, then there is the contraction that plays the role of the effuse, at the end of a long pipe it is placed the test section that is outside the wind tunnel. This type of configuration is not so spread due to the

positioning of the test section, being outside the wind tunnel all the measurements acquired are highly dependent on the external conditions.

The second member of the family of the wind tunnel is the closed loop. The closed loop configuration is more complicated than the open loop and also bulkier but it offers a higher quality of the flow and more controlled. All the variables that can affect the measurements can be controlled and changed during the operation, so there is no more a link with the external conditions. Less energy is required to run an experiment thanks to the pressure recovery in the diffuser. The installation of heat exchangers is needed in order to cool down the flow, in fact being continuously inside the loop at a certain velocity due to the skin friction the flow tents to heat up, changing the density and the pressure. In order to keep constant the variables during the operations it is necessary to cool down the flow. In this case in order to reduce the length of the diffuser expanding corners can be adopted. The expanding corners have an outlet area greater than the inlet one, they need guide vanes in order to direct correctly the flow without face separation; usually the guide vanes are 3D airfoil. Using expanding corners the circuit length of the wind tunnel can be reduced up to 20%for a given test section. Prior the stagnation camber layers of honeycomb and screens are installed. The role of these layers is to create a homogeneous, uniformly directed and constant velocity profile. The presence of screens and honeycomb

(a) *Wind tunnel*

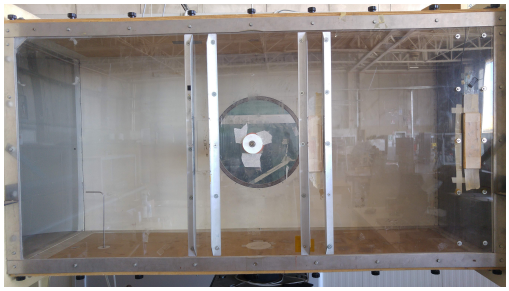

(b) *Test section*

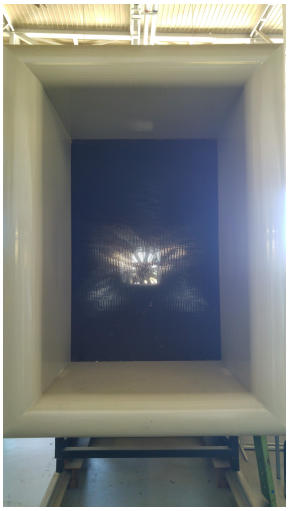

(c) *Inlet of the wind tunnel*

(d) *Exit section of the diffuser*

Figure 3.1: *Main features of the wind tunnel used for this study. One wall of the test section is made of plexiglass in order to be able to see what is happening inside, in the opposite wall there is a rounded window from which is possible change the set up inside the test section. The image of the inlet shows the presence of screens and honeycombs, that guarantee the creation of a laminar and organized flow. Being a suction open loop wind tunnel, the fan is installed at the exit of the diffuser as shows the last image..*

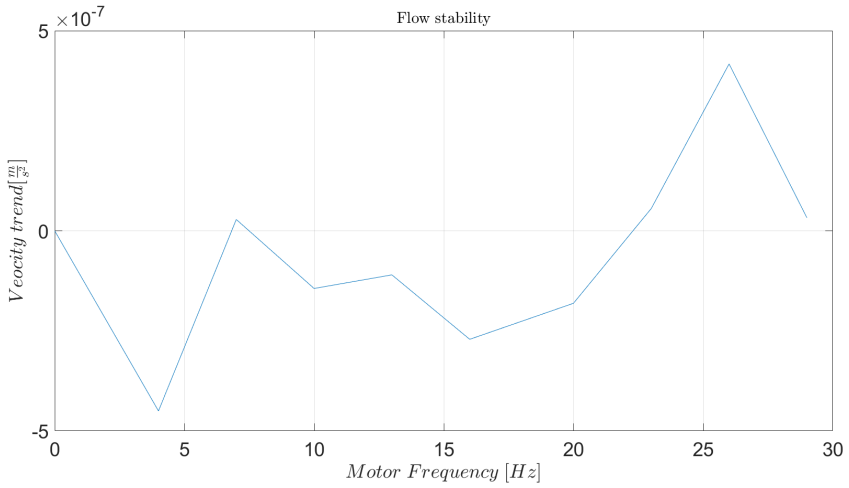

Figure 3.2: *Velocity tendency of the flow inside the wind tunnel for different values of velocity. It can be seen that the variation of velocity is of the order of* $10^{-}7$*, thus can be considered negligible.*

involves a large pressure drop, usually it is preferred the installation of a cascade of screens rather than a single screen with equal pressure drop.

For the experiments the wind tunnel has a test section with these dimensions:$180x90x60$ with rectangular cross section. In on wall of the test section three rectangular holes are placed in order to measure the flow in different region. The inlet consists in a rectangular section with the size of $150x225$. One layer of honeycomb is installed with a cascade of three screens. The settling chamber has a length of 70cm, then is placed the contraction. Here the cross section dimension is reduced up to the one of the test section. After the test section there is the diffuser with circular section. The diameter in the exit section is equal to 252cm. The overall length of the diffuser is 11 meters

The analysis of the quality of the flow inside the wind tunnel shows the following results. The figure shows how the flow velocity changes in time for a given velocity. The values were obtained approximating the signal in time with a linear curve (using least square approach), and then the information was extrapolated from the slope of the linear curve. No great peaks are visible and are all in the order of 10^{-7} so the flow can be considered stable in time. The following table shows the standard deviation evaluated for every velocity measured

Frequency [Hz]	Mean velocity[m/s]	Standard deviation
4	1.90	0.032
7	3.91	0.195
10	5.97	0.020
13	8.09	0.020
16	10.2	0.025
20	13.1	0.027
23	15.3	0.051
26	17.6	0.032
29	19.8	0.032

Table 3.1: *Value of standard deviation for each velocity. For all the velocities the value of the standard deviation is very small, this is another indicator of the good quality of the flow.*

Being the standard deviation an indicator of how much the data are spread from the mean (as expressed in the previous chapter), it can be seen as a parameter linked to the turbulence level inside the wind tunnel.

These results were obtained using the Pitot probe, that was fixed in a certain position inside the wind tunnel (bottom half of the cross section of the test section). The quality of the flow was also studied in space and not only in time. This step was made through the use of the hot wire. The acquisition were made in the centreline and top half of the test section. The results show a little difference in the velocity, thus the flow can be considered homogeneous also in space. This study was necessary in order to understand the quality of the flow and if the wind tunnel had critical velocities in which the flow can be unstable or separate. Be aware of the characteristic of the flow means better comprehend the results obtained in the future experiments.

Frequency [Hz]	Velocity [m/s]	
	Up	Center
4	1.64	1.60
10	5.20	5.26
16	9.94	9.70
29	19.1	19.3

Table 3.2: *Evaluation of the velocity inside the test section of the wind tunnel in two different points. The values are almost the same, it can be said that the flow can be considered homogeneous in space*

3.2 The Pitot probe

One of the most important tool in this type of experiment is the Pitot probe. The Pitot probe is necessary to measure the velocity of the flow inside the wind-tunnel. It measures the speed starting form the pressure measurement, thanks to two hole placed one in the stagnation point (total pressure) and one on the surface of the probe (static pressure). The relation between pressure and velocity is given by the Bernoulli equation: the total pressure is equal to the dynamic pressure and static one. Once it is known the total pressure and the static pressure it can be obtain the speed that is inside the dynamic pressure:

$$P_t = P_s + P_d \tag{3.1}$$

$$P_t = P_s + \frac{\rho V^2}{2} \tag{3.2}$$

$$V = \sqrt{\frac{2\left(P_t - P_s\right)}{\rho}} \tag{3.3}$$

The Pitot probes are useful to measure the main mode of the flow because it has a low dynamic response, for this reason it is mainly adopted to measure the main velocity. During the installation inside the wind tunnel, it must be pay close attention to the axial direction of the probe with respect to the flow. The Pitot probe in fact has a great directional sensitivity and some degrees of misalignment can produce wrong results.

Regarding the total pressure hole it must be paid attention on the shape of the velocity profile, in fact if the flow it is not homogeneous in the direction orthogonal to the probe axis some corrections must be applied. This because it was found that the flow particles measured are not the one who lays in that given coordinate but they are shifted down a

little. The opposite phenomenon happens in the case of wall interference. In the case of a velocity gradient there exist three different corrections obtained empirically.

$$\frac{\Delta y}{d} = \epsilon \quad \epsilon = 0.15 \tag{3.4}$$

$$\frac{\Delta y}{d} = 0.18\alpha\left(1 - 0.17\alpha^2\right) \quad \alpha = \frac{d}{2U\left(y_c\right)}\frac{dU}{dy} \tag{3.5}$$

$$\frac{\Delta y}{d} = 0.15 \tanh 4\sqrt{\alpha} \tag{3.6}$$

These are based on analytical displacement correction for a sphere in a velocity gradient.[15] In the case of wall interference, instead:

$$\delta_w = \epsilon d_p \tag{3.7}$$

With d_p that is the diameter of the probe. Depending on the distance of the probe to the wall ϵ has different values:

$$\begin{cases} \epsilon = 0.150 & d^+ < 8 \\ 0.120 & 8 < d^+ < 110 \\ 0.085 & 110 < d^+ < 1600 \end{cases} \tag{3.8}$$

In this study none of these corrections were necessary because the measurements were done in far from the wall and in absence of any velocity gradient. Also the static port can have some bad readings, these errors can be due to: orifice shape, orifice orientation, depth of the cavity and the surface orientation.

In order to look at all the quantities that can affect a bad reading on the static port a PI group is created:

$$\Pi = \frac{\Delta p}{\tau_w} = f\left(\frac{d_s u_\tau}{\nu}, \frac{d_s}{D}, M, \frac{l_s}{d_s}, \frac{d_c}{d_s}, \frac{\varepsilon}{d_s}\right) \tag{3.9}$$

to reduce the errors it is important to work with these quantities, or at least with the most of them.

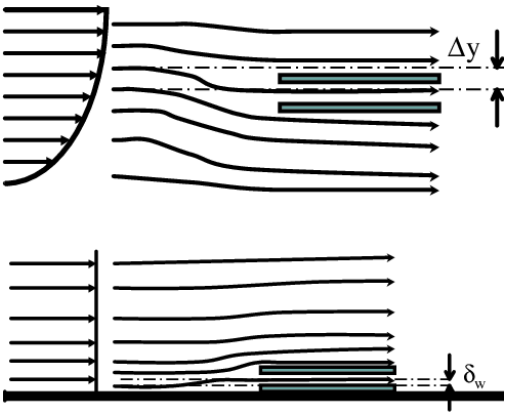

Figure 3.3: *B.J.McKeon, J.Li [15]Two type of Pitot total port interference: velocity gradient and wall interference. In the first case the flow particle shift down, so the velocity read is higher than the real one, the opposite happens in the second case.*

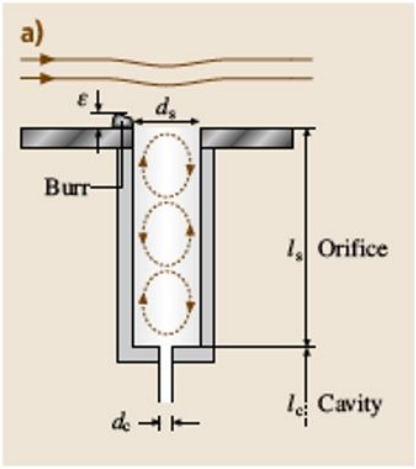

Figure 3.4: *G.Bellani, A.Talamelli, Lecture notes [16]. Sketch of the static port in a Pitot probe. There exist lot of variable that can interfere with the reading of the signal. It is very important to understand how the error can be reduced.*

3.3 The hot-wire

The hot-wire is another tool useful to study the velocity of the flow in consideration. Unlike the Pitot probe, the hot wire has a much larger dynamic response, for this reason it is used in order to study fluctuation of the flow in the turbulent regime. The hot-wire consists in a tiny resistance connected to an arm of a Wheatstone bridge. Prior any experiments the calibration of the hot wire is necessary. Despite the Pitot probe that does not require any calibration because the reading of the pressure measurements gives immediately the values of the velocity, the hot wire needs to be calibrate in order to link any values of the output voltage to the velocity. The process of calibration starts with the evaluation of the resistance of the anemometer. The resistance of the anemometer is evaluated by subtracting the value of the resistance of the cable and Wheaston brdige, obtained by introducing a shortening probe, to the overall system: hot-wire, cable and Wheastone bridge. This first step is essential considering that due to the aging effect the value of the resistance can change, obtaining wrong measurements. Once the resistance has been evaluated different measure at different velocities are made. A key factor is to place close to each other the Pitot probe and the hot wire in order to know exactly the value of the velocity. After several measurements at different velocity, through an interpolation by point it is obtained the calibration curve that links the voltage and the velocity. The main drawback of the Pitot probe is its behaviour at low velocities, it has an offset that tents to disappear as the velocity increases. This is shown in the calibration curve, in fact it starts from a velocity equal to 0.6 m/s. This aspect is felt in the results in the regions where the velocity is low.

The physics behind the functioning of this device is related to the Joule effect: a current flows through a resistance that heats up, when this resistance is exposed to a flow there will be a heat loss due to convection, radiation and conduction; know the amount of heat lost means know the velocity of the flow. As already said the three main component that cause the heat loss are: convection, it plays the main role, conduction and radiation are very small with respect the other one and sometimes they can be considered negligible. The governing equation is:

$$\frac{dE}{dt} = W - H \tag{3.10}$$

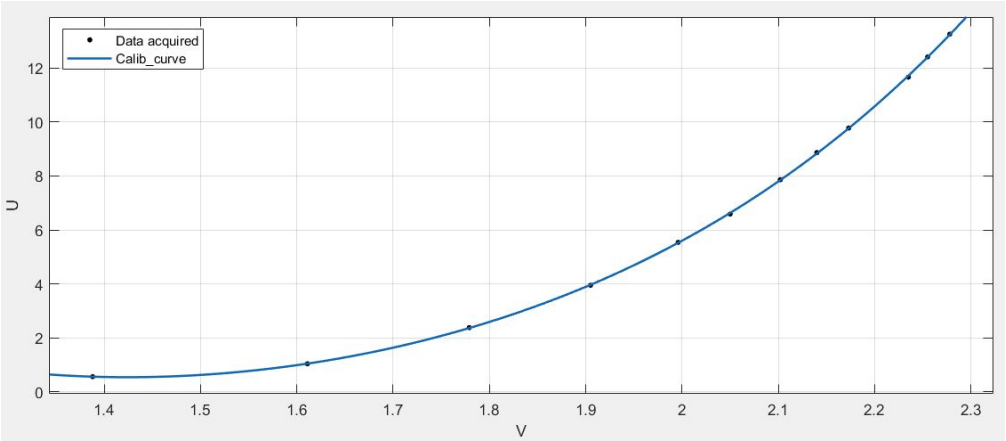

Figure 3.5: *Hot wire calibration curve obtained interpolating a 4th polynomial curve.*

dE/dt=W-H Where $E = C_w T_s$ and $W = I^2 R_w$. E is the thermal energy stored in the wire and it is defined as the product between the heat capacity of the wire and the temperature; W is the power generating by the Joule effect and it is defined as the square of the current times the resistance of the wire, that is a function of the temperature of the wire itself[14]. The overall system is in equilibrium when $W = H$. In particular, defining T_a as the ambient temperature and knowing that $I = \frac{V}{R_w}$:

$$W = H \tag{3.11}$$

$$\frac{V^2}{R_w} = hA_w\left(T_w - T_a\right) \tag{3.12}$$

the previous expression can be written by introducing a dimensionless number: the Nusselt number $Nu = \frac{hd}{k}$.

$$\frac{V^2}{R_w} = kNu\frac{A_w}{d}\left(T_w - T_a\right) \tag{3.13}$$

where k is the thermal conductivity of the fluid and d the characteristic length of the body, in this case the diameter of the wire. The Nusselt number is a function of several quantities:

$$Nu = Nu\left(Re, Pr, M.\tau, \dots\right) \tag{3.14}$$

Where

$$Re = \frac{U d \rho}{\mu}; \quad Pr = \frac{c_p \mu}{k}; \quad M = \frac{U}{a}; \quad \tau = \frac{T_w - T_r}{T_0} \tag{3.15}$$

τ is called overheat ratio, with T_r that is the recovery temperature and T_0 the stagnation temperature. The relation that links all these variables is known as the King's law and it is written as:

$$Nu = A'\left(\tau\right) + B'\left(\tau\right)Re^n \tag{3.16}$$

Combining this expression with the one obtained in the previous equation it is obtained the equation for the calibration of the sensor:

$$V^2 = A\left(\tau\right) + B\left(\tau\right)Re^n \tag{3.17}$$

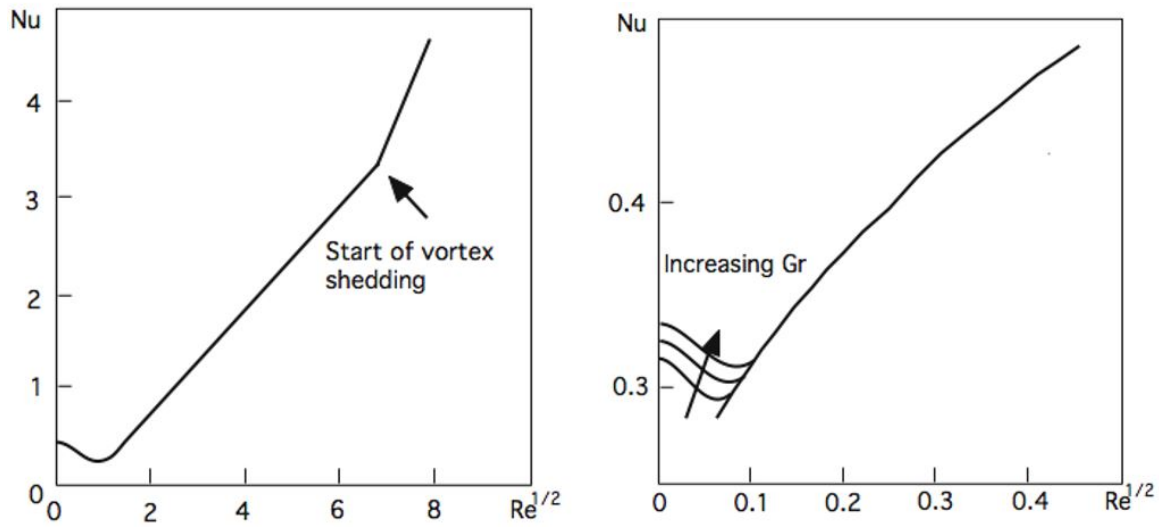

Figure 3.6: *G.Bellani, A.Talamelli, Lecture notes [16].Relation between Nu and Re. At very low Reynolds number the relation is dependent on the Grashof number.*

The exponent n is in the range of 0.4/0.55. It is interesting to look at the relation between the Nusselt number and the Reynolds number.

$$Gr = \frac{g\beta D^3 \left(T_s - T_{\inf}\right)}{\nu^2} \tag{3.18}$$

The Grashof number is a dimensionless number and it is the ratio between buoyancy and viscous force acting on a fluid. g is the gravity acceleration, β is the coefficient of thermal expansion of the wire, D the diameter of the wire, T_s the temperature of the wire and $T_{\inf}$ the temperature of the environment and ν is the kinematic viscosity of the fluid. If very low Reynolds number are reached it is possible to face some buoyancy effect, in order to avoid it the Reynolds number must be at least one third greater than the Grashof number. In standard case this means have a velocity greater than 0.07m/s.[16]

As well as the Pitot probe, also the hot wire anemometer is directional sensitive. It must be paid attention on the direction of the sensor with respect the flow. There are two coefficients that takes into account the yaw (θ) and pitch (α) components of the velocity:

$$U_{eff}^2 = U_x^2 + k^2 U_y^2 + h^2 U_z^2 \tag{3.19}$$

This velocity is called “effective cooling velocity”, that is different from the velocity acquired in the computer, in fact the velocity acquired is the perpendicular component of the velocity. The previous expression was found taking the components of the velocity in the normal and tangential plane with respect to the wire. In the case of x-y plane, the angular response is characterized by a strong decrease of effective velocity when the angle α increases. This can be explained thanks to the heat transfer of a cylinder, the heat transfer is highest when the flow is normal to the cylinder. This is called Champagne law:

$$U_{eff}^2 = U^2 \left(\cos\alpha^2 + k^2 \sin\alpha^2\right) = U_x^2 + k^2 U_y^2 \tag{3.20}$$

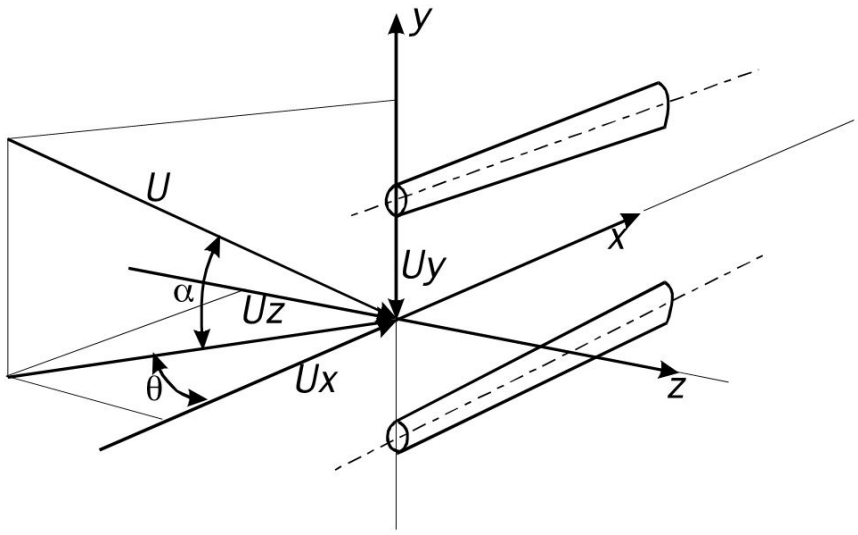

Figure 3.7: *G.Bellani, A.Talamelli, Lecture notes [16]. Directional sensitivity of the hot wire anemometer. The yaw and pitch angle are the ones that can affect the reading of the signal.*

In the x-z plane the angular response is expressed by Gilmore:

$$U_{eff}^2 = U^2\left(\cos\theta^2 + h^2 \sin\theta^2\right) = U_x^2 + h^2 U_z^2 \tag{3.21}$$

Usually the value of k is around 0.1, regarding h it is in the range between 1 and 1.1. This is due to the effect of the wire prongs that, in case of binomial direction of the flow, cause an acceleration of the flow in the location of the wire. The family of the hot-wire can be divided in three groups depending on the principle of functioning: Constant Current Anemometer (CCA), Constant Voltage Anemometer (CVA) and Constant Temperature Anemometer (CTA). As the name suggests, the CCA keeps the current constant through the sensor. This type of Hot-wire is not so spread, it has several drawbacks such as: highly risk of probe burnout, low frequency response and the output of the sensor decrease with the increasing of the velocity. The main advantage of this configuration is the low level of noise. The CVA keeps constant the voltage through the sensor, it has a large response and high frequency response. The CTA keeps the temperature constant, it is the configuration adopted for this experiment. It has a great dynamic response but it is very susceptible to the noise. The frequency response of the CTA is determined by the square wave test. The hot wire receives a train of square waves, depending on the settling time (time in which the signal returns in the previous configuration) the frequency response is determined. Regarding the CCA the frequency response can be obtained by:

$$M = \frac{c_w \rho_w \alpha_R d^2}{k_f Nu} \tag{3.22}$$

Where $c_w$is the heat capacity of the wire, ρ_w is the density of the wire material, $\alpha_R$is the thermal coefficient of the wire, d is the diameter, and Nu is the Nusselt number, k_f is the thermal conductivity.

(a) *Hot wire* (b) *Shortening probe*

Figure 3.8: *The shortening probe it is necessary to evaluate the value of the resistance of the Wheaston bridge and the cable. Once the hot wire is installed in order to compute the value of the resistance of the sensor it must be subtract the value of the new value of the resistance (Wheaston bridge+cable+HW) to the value previosly calculated.*

Considering that the velocity on which the experiments were performed were much higher than the minimum velocity needed in order to take into account the buoyancy effect, the correction in the calibration curve using the Grashof number was not implemented. Also the correction on the orientation was avoided because in the wake the direction of the flow is chaotic, moreover this study deals with the evaluation of the spctrum and this does not effect the evaluation of the shedding frequency, it effects only the balue of the energy associateted to it.

Chapter 4

Experimental set up

Figure 3.8 shows the hot wire anemometer used in both the cylinder and wheel with a filament made of platinum. Also the traverse system (figure 4.1) was the same in both cases and the Pitot probe. In the case of the wheel the installation of a wooden plate was necessary in order to simulate the ground. In both cylinder and wheel it was not used the balance due to the low velocity of the experiments, the drag obtained in fact was in the order of the scale error. To calibrate the hot wire is necessary the presence of a Pitot tube, which is positioned in front of the test section, in order to measure the free stream velocity with less disturbance possible.

4.1 The cylinder

Before showing the results of the 2D cylinder, it is important to illustrate to the reader the experimental set up. The hot wire was installed into a traverse system capable to cover all the points in the wind tunnel test section by changing the angle with respect the horizontal axis and its length from one of the two walls of the test section. In particular 18 acquisition points were studied, as the following image shows. The cylinder adopted has a diameter of 80mm and a length equals to the width of the cross section, in this way it is simulated the 2D world. No presence of 3D vortices is felt. Two main types of experiments were carried on. One was focused on changing the vertical position of the sensor keeping the same velocity, in this case it is possible to reproduce the mean velocity profile of the cylinder and understand

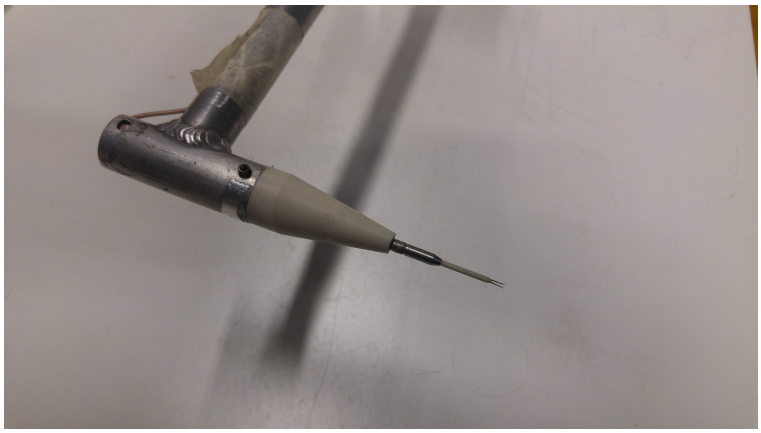

Figure 4.1: *Close up of the hot wire installed on the traverse system.*

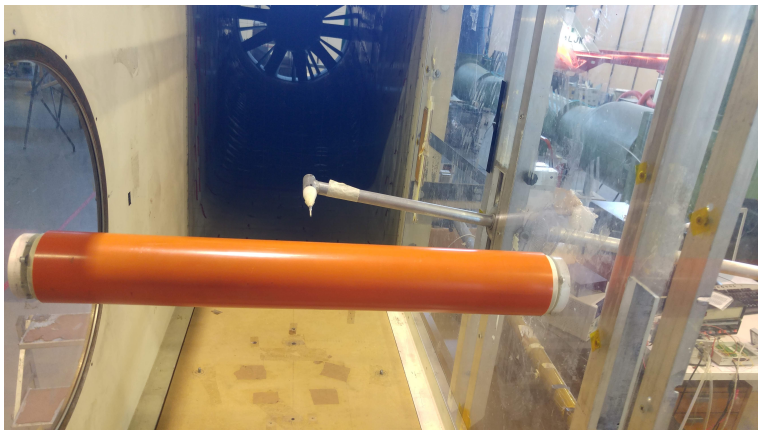

Figure 4.2: *Cylinder set up. Here it is shown the cylinder in exam having a diameter of 8cm and length of 58cm. On the back it is present the hot wire anemometer installed on the traverse system.*

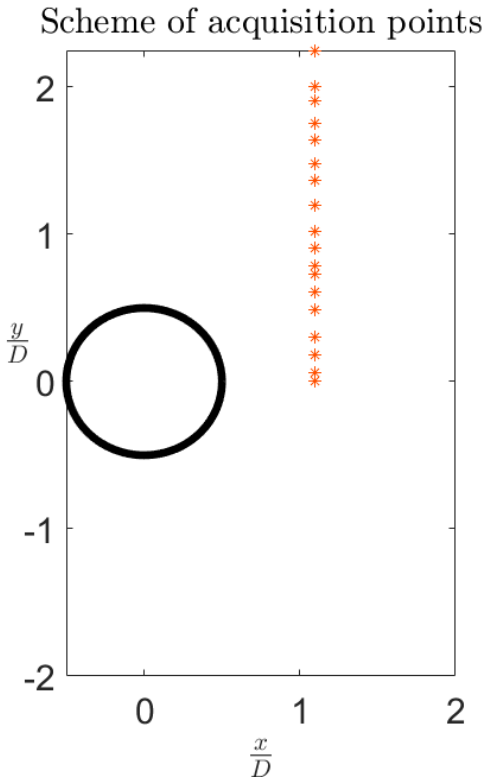

Figure 4.3: *Scheme of acquisition points for the study of the cylinder.*

some features of its wake. The second one was focused on keeping the hot wire in the same position and changing the velocity in order to see how the vortex shedding changes and its relationship with the velocity. The experiments were conducted at a velocity equal to 10m/s with a sempling frequency equal to 1500Hz. The time of acquisition was set to 120 seconds.

4.2 The wheel

Regarding the wheel experiments the installation of the ground was paramount, in particular this is necessary in order to avoid an excessive growth of the boundary layer. On this plate it was cut an eyelet permitting the study of the wake in different distance from the wheel, since the hot wire support is fixed, it was necessary to move the wheel. To be sure that the flow does not separate on the leading edge of the plate a flap was positioned on the back of the ground. Changing the incidence of the flap the direction of the velocity changes as well. On the leading edge there were put some strings in order to understand the behaviour of the flow in that position. If the strings had moved chaotically it would have meant that the flow separated, to make the flow attached to the ground it must move the flap until the stripes start being parallel to the ground axis. This procedure it is very important because affects drastically on the results, it can happen that if the flow is oriented in a wrong way the wheel can lay inside the recirculation bubble and a complete different wake is observed.

Three type of wheels were studied in different configurations: wheel with sharp shoulders, wheel with 45 degrees shoulders and wheel with rounded shoulders. Totally there were acquired 130 points, 10 stations in the vertical direction and in each direction 13 points in the spanwise direction, a scheme of the acqusition points can be found in the following images. The acqusiition time in each point was 40 seconds with a sampling frequency of 300 Hz. Since the wheel with sharp shoulder it has no application on the automotive field it was only used as comparison for the other two cases and it was evaluated its wake only in a single distance. The 45 degrees and the rounded one were studied at different distances (z/D=1.45;2.25;2.65;3.05;3.45;3.85). Then a particular focus was given to the rounded wheel. In particular it was studied the wheel in two different stations (z/D=2.25;3.85) with a camber angle first and a camber plus a toe angle later. The value of these angles were decided on the value adopted in F1, a camber angle equal to -3.5° and a toe angle equal to -0.5°.

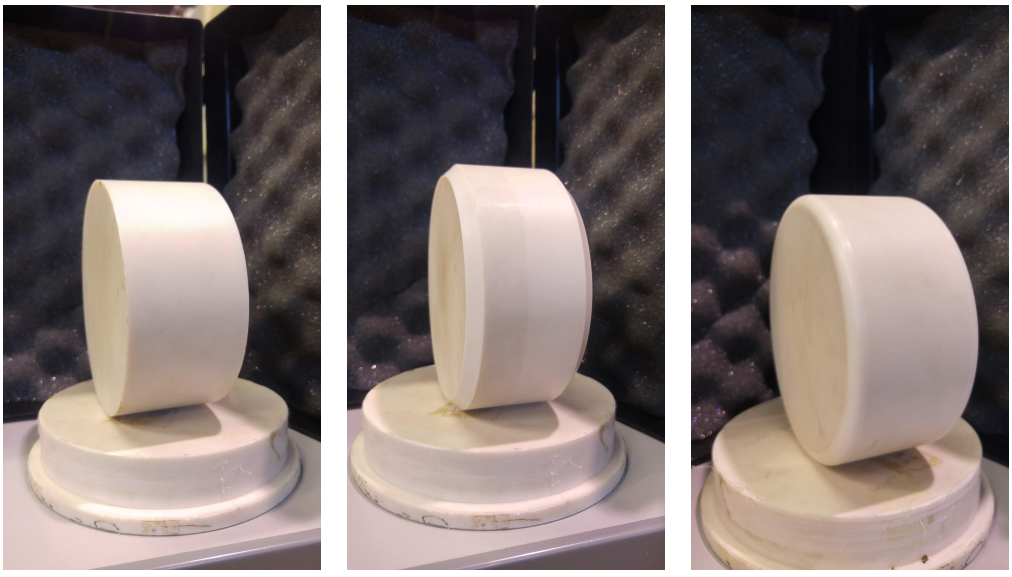

(a) (b)

Figure 4.4: *The three different types of wheel studied. On the lest there is the wheel with the sharp shoulder, in the centre the one with edges at 45 degrees and on the right the one with rounded shoulder.*

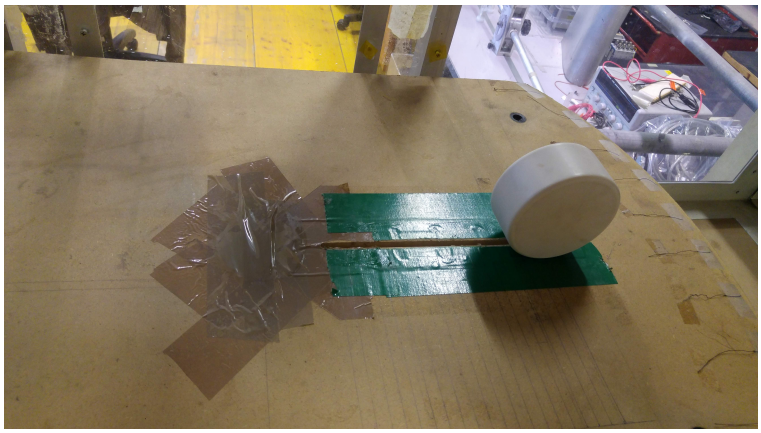

(a)

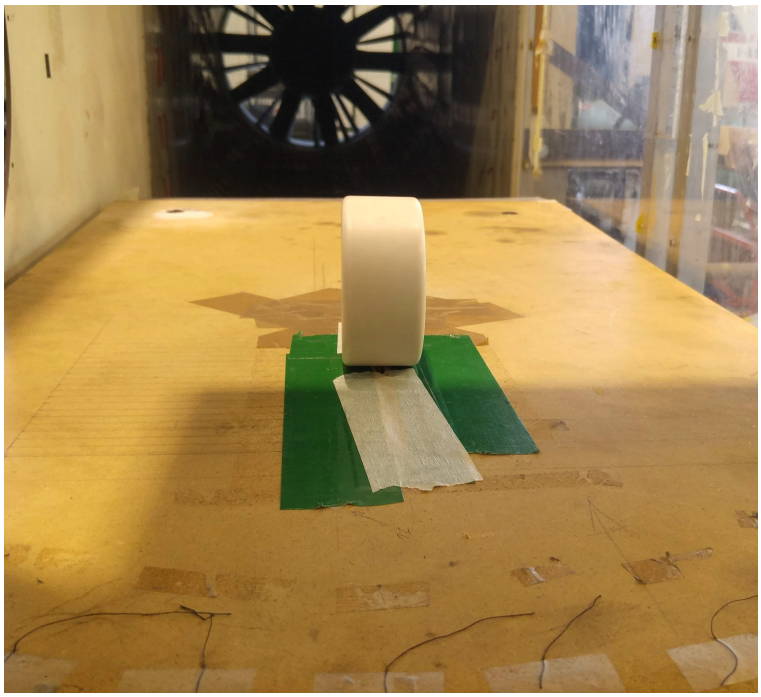

(b)

Figure 4.5: *Example of installation of the wheel on the ground. Thanks to the eyelet the wheel can be moved back and forth in order to evaluate the wake at different positions. Before every acquisition the eyelet is covered by a layer of tape in order to do no permit the air to flow under the ground.*

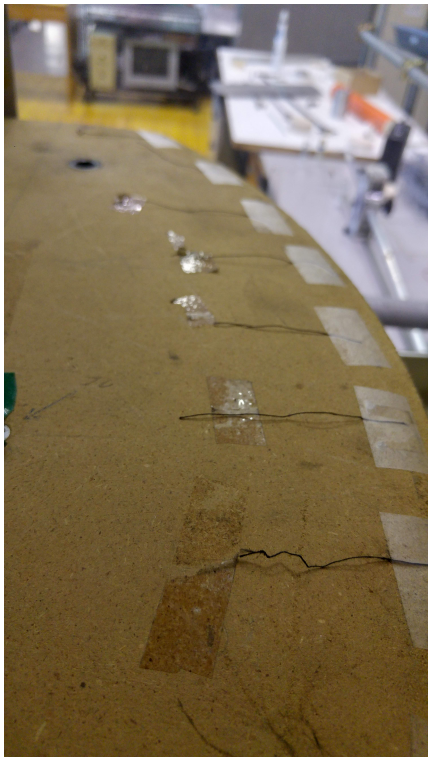

Figure 4.6: *Close up of the strips. When the flow is attached the stripes are steady and directed as the longitudinal axis of the ground. If the flow separates on the leading edge the strips will move chaotically.*

Figure 4.7: *Installation of the traverse system on the wind tunnel. By moving the traverse back and forth and inclining it with respect the horizontal plane it is possible to cover all the points of a given plane.*

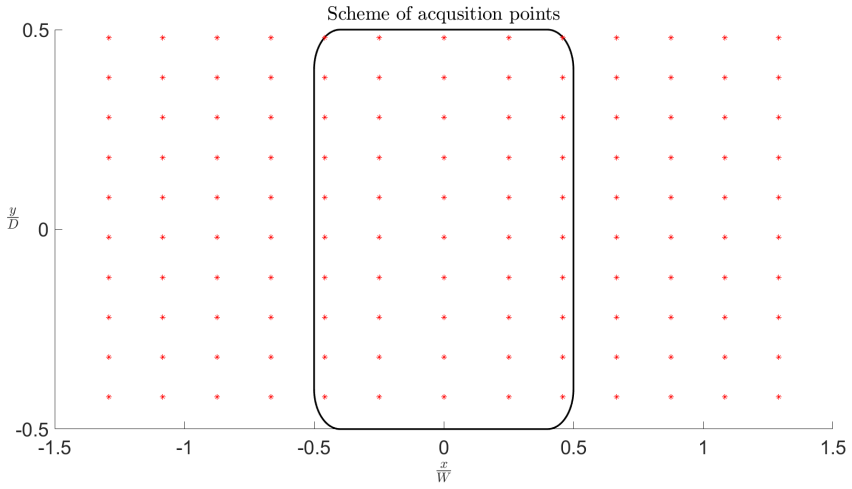

Figure 4.8: *Scheme of acquisition points for the study of the wheel wake.*

Chapter 5

Results

5.1 The cylinder

5.1.1 Wake features

From lectures of Guido Buresti[17] it can be found a relationship between the skewness and standard deviation value with the wake velocity profile. In particular the maximum value of the standard deviation coincides with the point in which it is felt the highest velocity gradient, while the minimum of the skewness reveals the wake boundary. These experiments were conducted only in a half part of the cylinder, assuming that the exact same shape can be obtained by mirroring the image. In the literature it was found a similar study conducted by Ong and Wallace[18]. Their study was the investigation of the turbulent wake near a cylinder. As in this experiment the data were acquired through and hot wire. The same process was made for the further station with x/D=8.8. Unfortunately, no data in the literature was found in order to make a comparison. The results are a little different than in the previous case. As before the minimum of the skewness underline the wake boundary but the maximum of the standard deviation does not fit with the highest

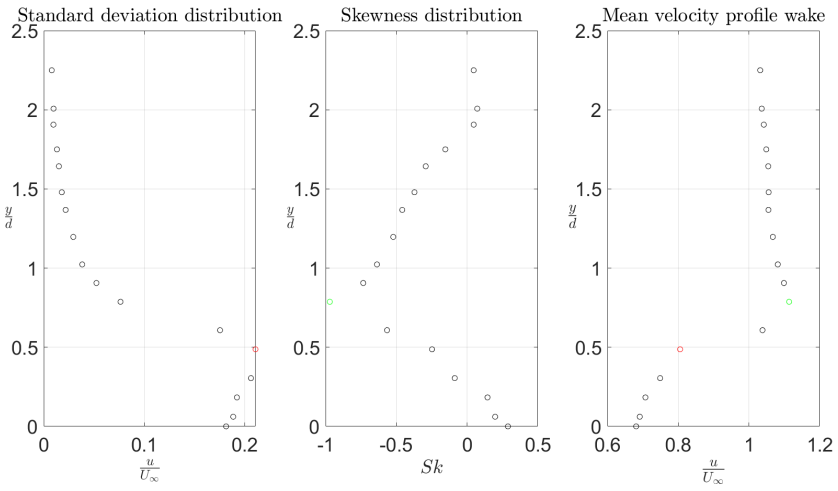

Figure 5.1: *On the left is represented the standard deviation value in the different acquisition points. In the centre it shown the skewness value of the different acquisition points. On the right it is shown the wake profile of the cylinder with D=0.8m, V=10 m/s evaluated in x/D=1.1.*

Figure 5.2: *Comparison of the results of the wake velocity profile behind a cylinder in x/D=1.1 between the actual data and the one obtained by Ong and Wallace[18]*

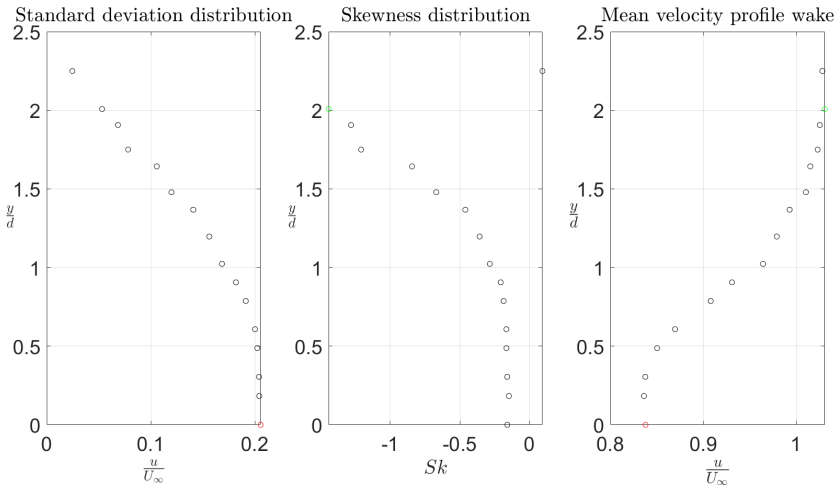

Figure 5.3: *Standard deviation, skewness and mean profile of the cylinder evaluated at x/D=8.8 with a velocity equals to 10 m/s. It can be seen that there is no more the relation between the maximum value of the standard deviation and the highest gradient. The skewness relation still holds true.*

gradient. This can be due to the high velocity fluctuation in the wake region. In fact now this point coincides with the wake centre.

As expected the wake profile tents to enlarge as the distance from the cylinder increases and the velocity deficit decreases. The comparison is shown in the following figure.

5.1.2 Spectral analysis

After the study of the mean velocity profile, the vortex shedding phenomenon has been investigated. The use of FFT is paramount in this case, the following results refers to the closer station with the same velocity as in the previous case, V=10 m/s. The results show an interesting aspect of the vortex shedding, inside the wake there exists two harmonics, while in the external region it exists only the main harmonic. This is due to the formation of the vortices that interact

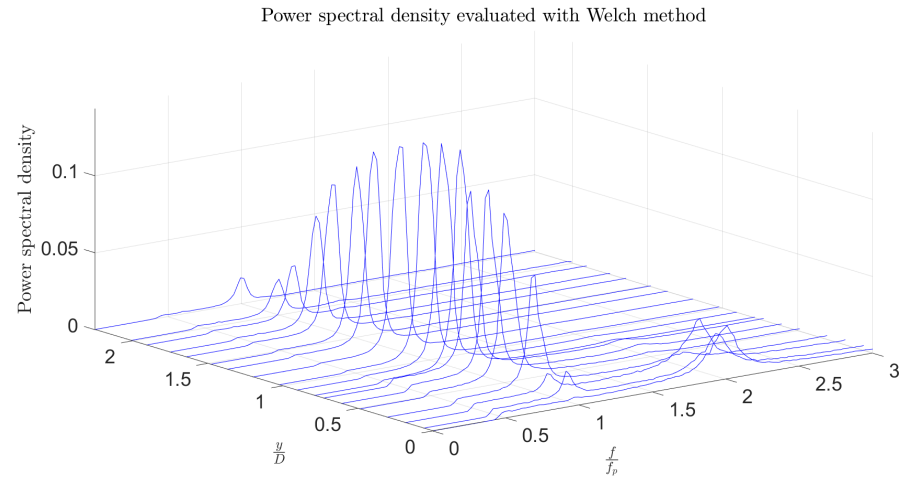

(a)

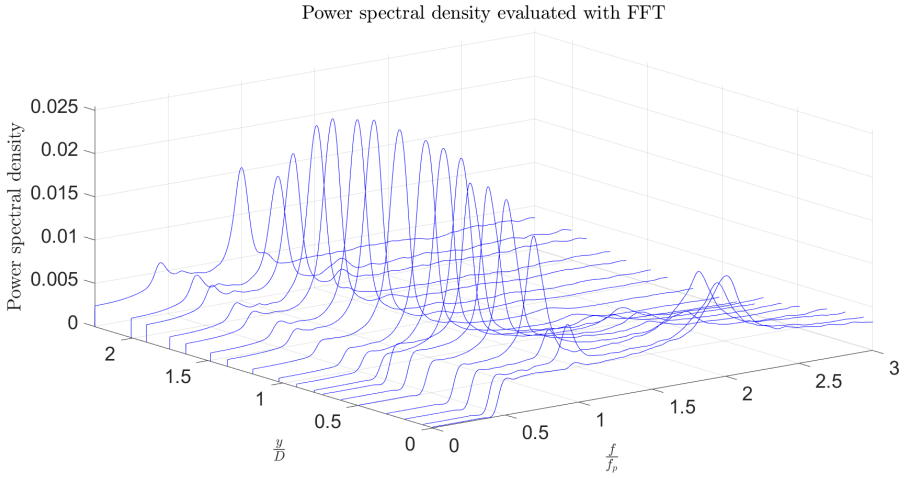

(b)

Figure 5.4: *Figure* a *shows the frequency spectrum in function of the shedding frequency, obtained through the Welch's method. Figure* b *shows the frequency spectrum in function of the shedding frequency, obtained through the FFT. The overshoot is much more visible in this case. The Welch's method reduces this effect by the usage of the windowing.*

with the sensor. The first graph represents the value of the signal frequency in the different positions, in particular the frequency is normalized by the shedding frequency that in this case is equal to 21.8 Hz. This results it was obtained thanks to the Welch's method. Using the normal FFT procedure it would have had a steeper graph in the cut off frequency points. A similar study was performed looking at the value of the shedding frequency in four fixed positions in the space and different velocities. In particular the hot wire was placed in y/D=0.18;0.42;0.6;0.9. The velocities values are U[m/s]=1.07;1.55;2;2.7;3.8;4.6;5.5;6.86;7.9;9.2;10. The evaluation of the spectrum was made by the using of the Welch's method, for low velocities the shape of the spectrum is more angular than for high velocities. It will be shown that the peaks shift to the right as the velocity increases and the value of the frequency in which the power is higher depends on the position of the hot wire. After having studied the behaviour of the shedding in different conditions of free stream velocity it was decided to see the relationship between the frequency and the velocity. As already explained in the previous section the relation between these two quantities is proportional to the Strouhal number and the characteristic

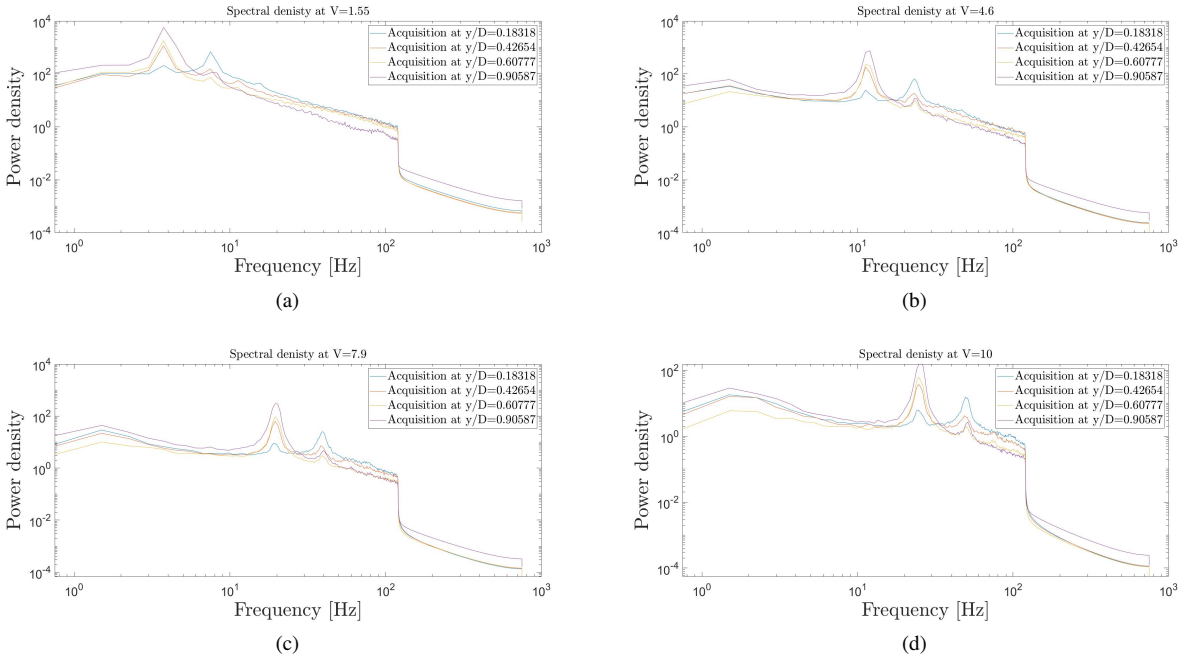

Figure 5.5: *Some examples of the velocity spectrum. In this case are reported four velocities:1.07;4;7;10 m/s. In each plot are present four spectra depending on the position of the hot wire. As it might be expected the peaks translates to the right as the velocity increases. Furthermore the second harmonic is more relevant in the case of y/D closer to the wake centre line.*

length of the body in exam (in this case the diameter). In particular this relation is linear and by plotting the graph Velocity/Frequency it can be evaluated the Strouhal number simply multiplying the angular coefficient of the line for the value of the diameter. The value of the St obtained is 0.197. Usually it varies in the range between 0.18 and 0.22 so it can be said that it is a good result.

In order to evaluate the results coming from the Pitot probe, it was focused on a different type of calibration of the hot wire. Usually the hot wire is calibrated, as explained in the theory, with the use of a Pitot probe. By looking at the value of the Pitot velocity signal and the voltage signal of the hot wire it is possible to draw a calibration curve (usually it is a 4th order polynomial curve). It is also possible to calibrate the hot wire using a cylinder and by looking at the frequency peaks inside the voltage signal, then take the value of the voltage in which is present the frequency peak and plotting the velocity/voltage plot (obtaining the velocity with a guessed Strouhal number). The results show a good overlap of the two calibration curves, mostly for the low velocities

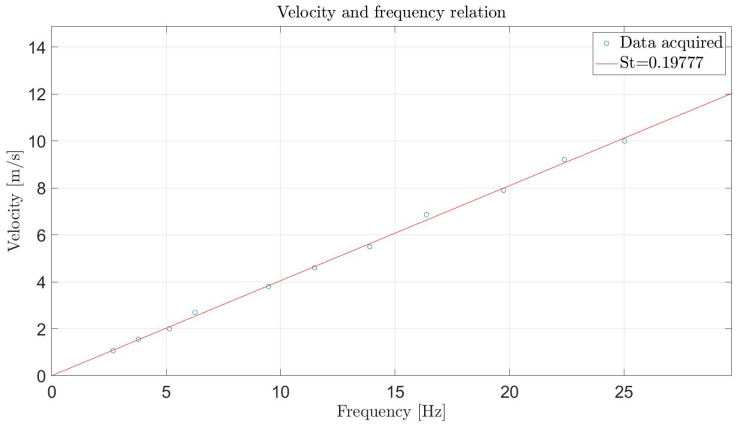

Figure 5.6: *Relationship between frequency and velocity. As expected from the theory it is a linear relationship proportional to the Strohual number and the diameter. The Strouhal obtained is 0.197.*

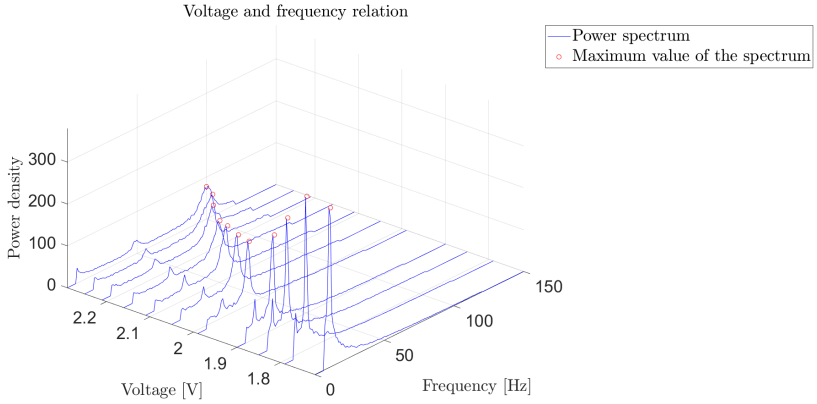

Figure 5.7: *Voltage and frequency relationship. For each voltage it is extracted the frequency in which it is present the highest peak.*

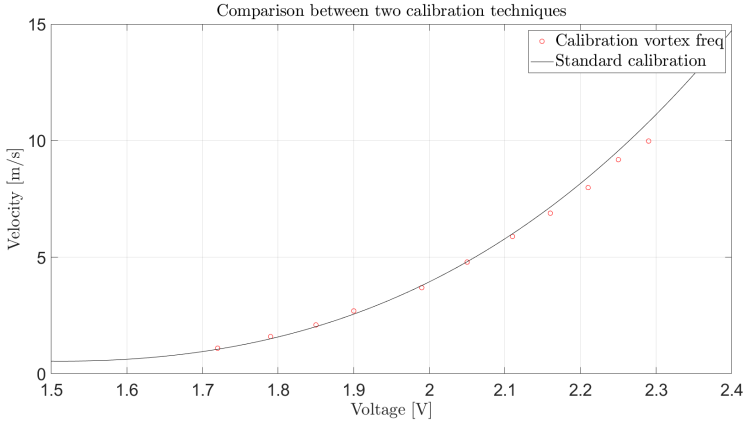

Figure 5.8: *Comparison between the two calibration curves. The one obtained in the non convential way it diverges a little from the standard one only at the higher velocities*

5.2 The wheel

5.2.1 Wake features

As already explained above, the study started with the comparison of the wake in a fixed distance from the wheel of the three type of bodies. In all plots there is a white strip all along the x axis where it was not possible to acquire the data due to the encumbance of the hot wire support. Considering that it is very difficult to predict the behaviour of the flow in that position it was decided to consider only the flow starting from $\frac{y}{D} = -0.42$. The plots show the velocity contour in z/D=1.45, in the x axis it is represented the wake width normalized by the width of the wheel. A big difference is visible between the wheel with sharp shoulders and the other two. While on the 45-degree and round shoulders it is clearly visible the presence of two main vortices coming from the top of the body to the ground having opposite value of vorticity, the sharp edge wheel has a wake as high as the wheel. This is an important result that underlines the effect of the shoulders, in fact looking at the shape of the wake it is possible to understand the impact of the shape on the drag. It is clear that the sharp shoulders wheel has an higher resistance rather than the 45 degrees or rounded one. Thanks to the shoulders infact, the flow can follow more the shape of the body, and in the process on doing that it creates those two big vortices visible in the figures. In the case of the sharp shoulders, the flow it is not able to follow the geometry of the body and detaches before, generating a larger wake. The next step was focused more on the round shoulder wheel, in particular on the changing of the wake shape by the variation of some parameters, such as the camber angle and toe angle. The wake was acquired in two different position: z/D=2.25 and z/D=3.85. It is interesting to see how the vortex on the right has a higher dimension rather than the one on the left. This result is similar to the one obtained by Robin Knowles, Alistair Saddington and Kevin Knowles [11]. They studied the influence of the camber angle on the wheel wake through the usage of the PIV technique, They found the presence of an asymmetry on the wake and in particular the presence of a bigger vortex in the portion of the wheel that it is more in contact with the ground. Later it was given to the wheel a toe angle equal to 0.5°. Unfortunately this value is very small and no big differences were observed. The only difference visible is on the left part of the wheel in z/D=2.25 where the wake is a little higher than in the case of only camber angle. This results is given by the orientation of the wheel with respect the direction of the velocity. Having a certain side angle, will bring the wake to have a more pronounced shape in a side of the wake itself rather than in another.

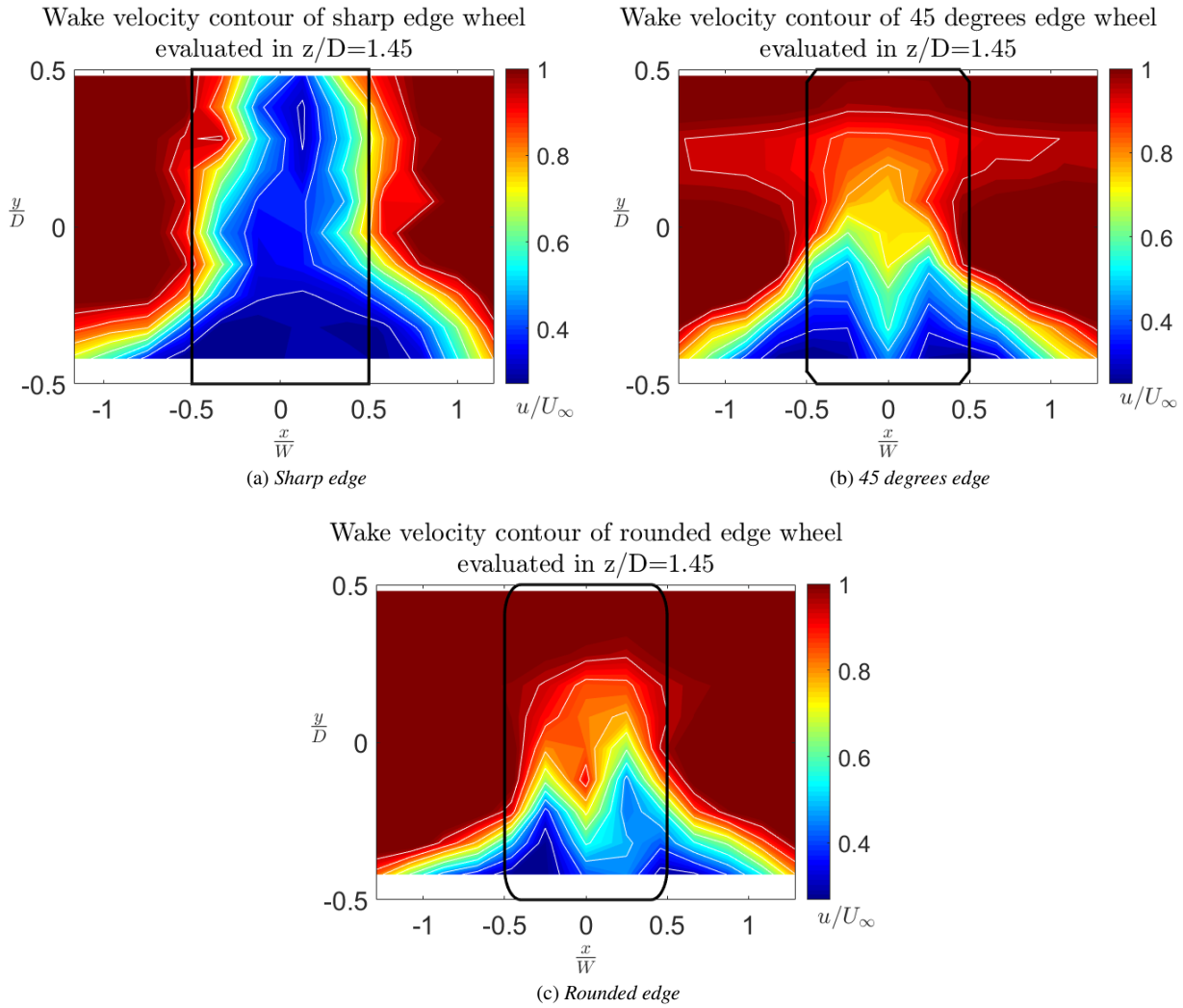

(a) *Sharp edge*

(b) *45 degrees edge*

(c) *Rounded edge*

Figure 5.9: *Velocity contour of the wake with different types of wheels. In the case* (a) *the wake is high as the wheel generating an higher resistance. In* (b) *the shape is completely different from the previous one and the presence of two big vortices can be seen. In* (c) *the shape is similar to the one with 45 degrees. The main difference is on the top region of the wake where it seems to be more compact and organized. The lower peaks on the right can be due to a wrong positioning of the hot wire*

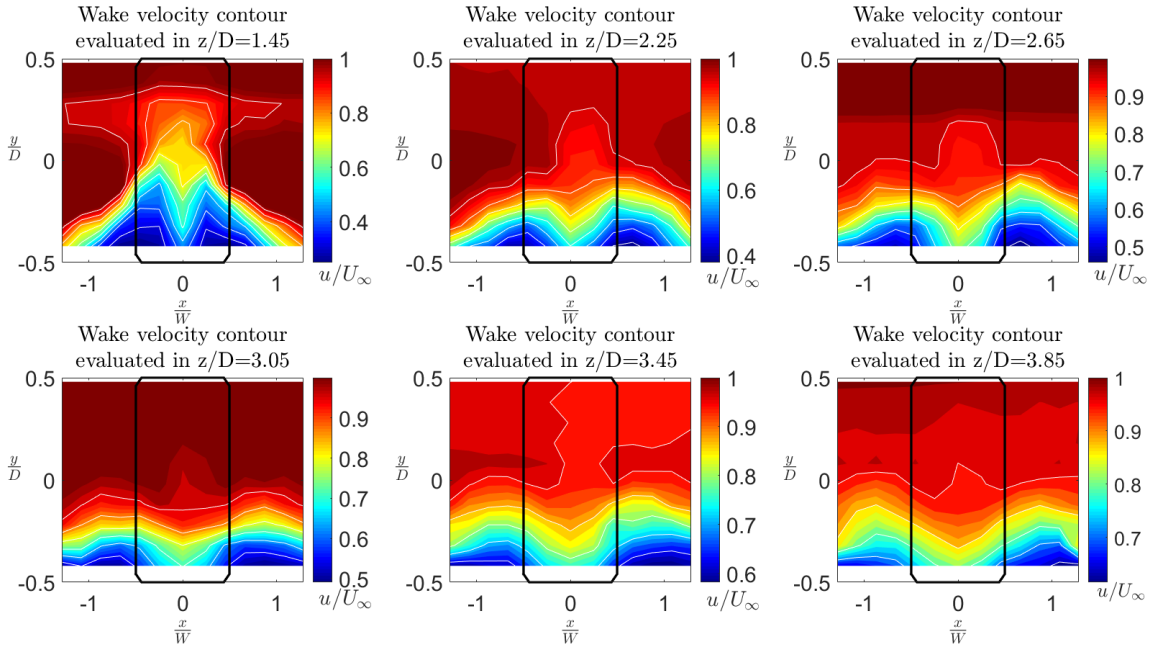

Figure 5.10: *Evolution of the wake in the case of the wheel with 45 degrees shoulder. As the distance increases the wake enlarges and becomes flatter.*

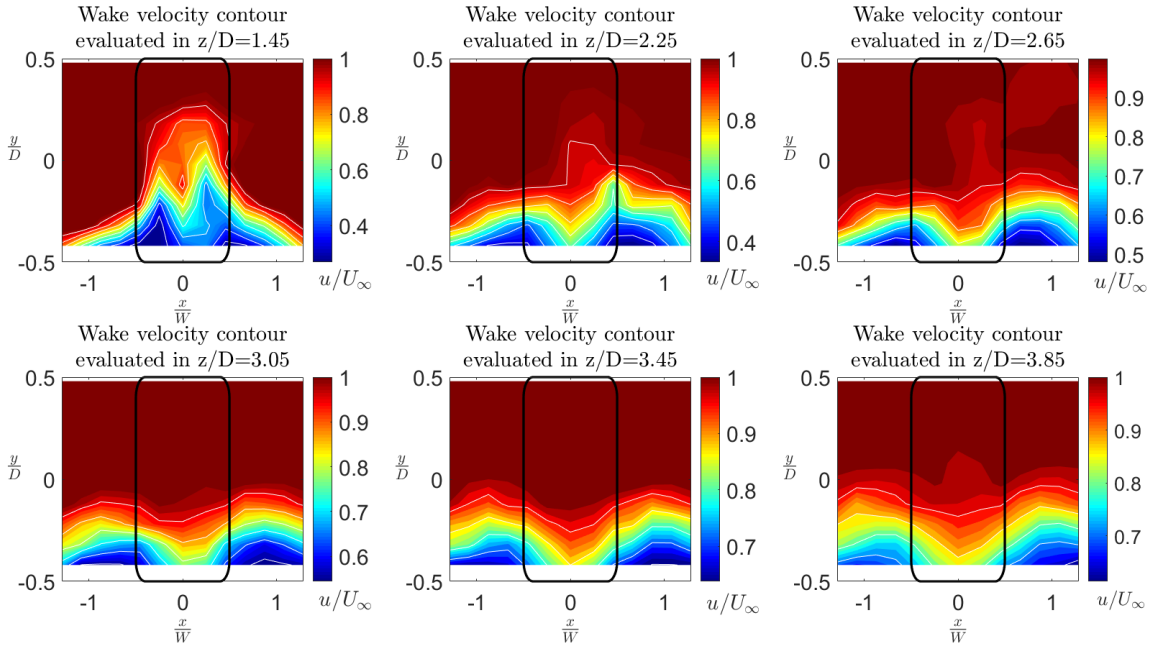

Figure 5.11: *Evaluation of the wake in the case of the wheel with rounded shoulder. The behaviour is very similar to the one obtained in the previous case, where the wake becomes flatter and larger as the distance increases.*

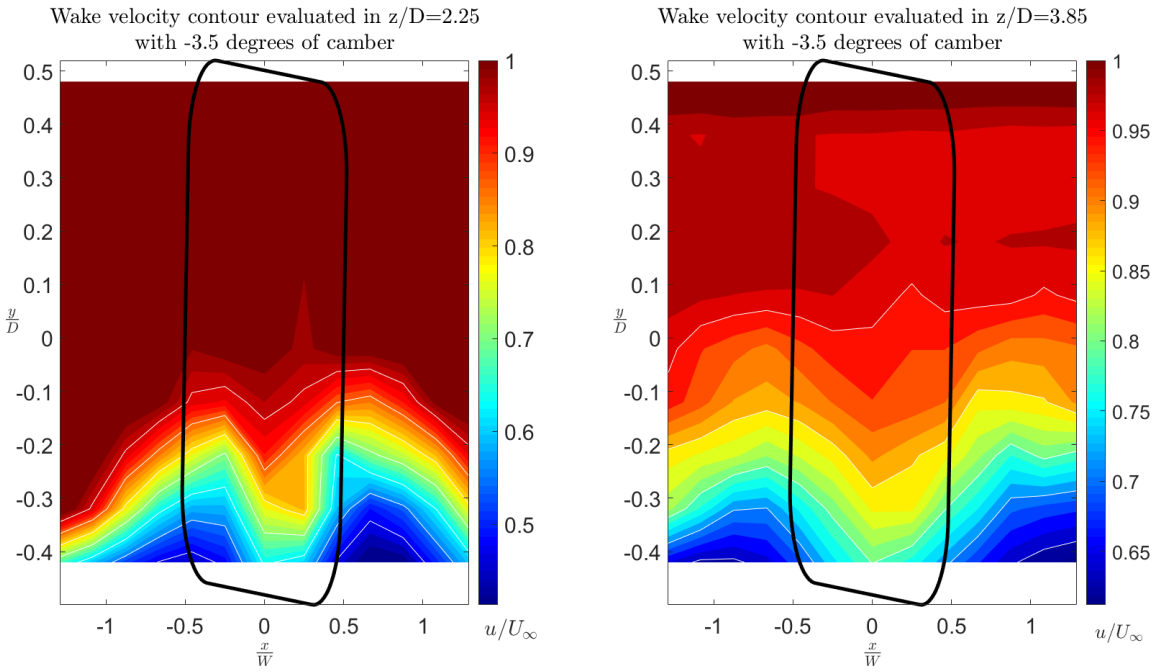

Figure 5.12: *Wake of cambered round shoulder wheel at two different distances. On the left z/D=2.25 one the rigth z/D=3.85. The camber angle has been set to -3.5*

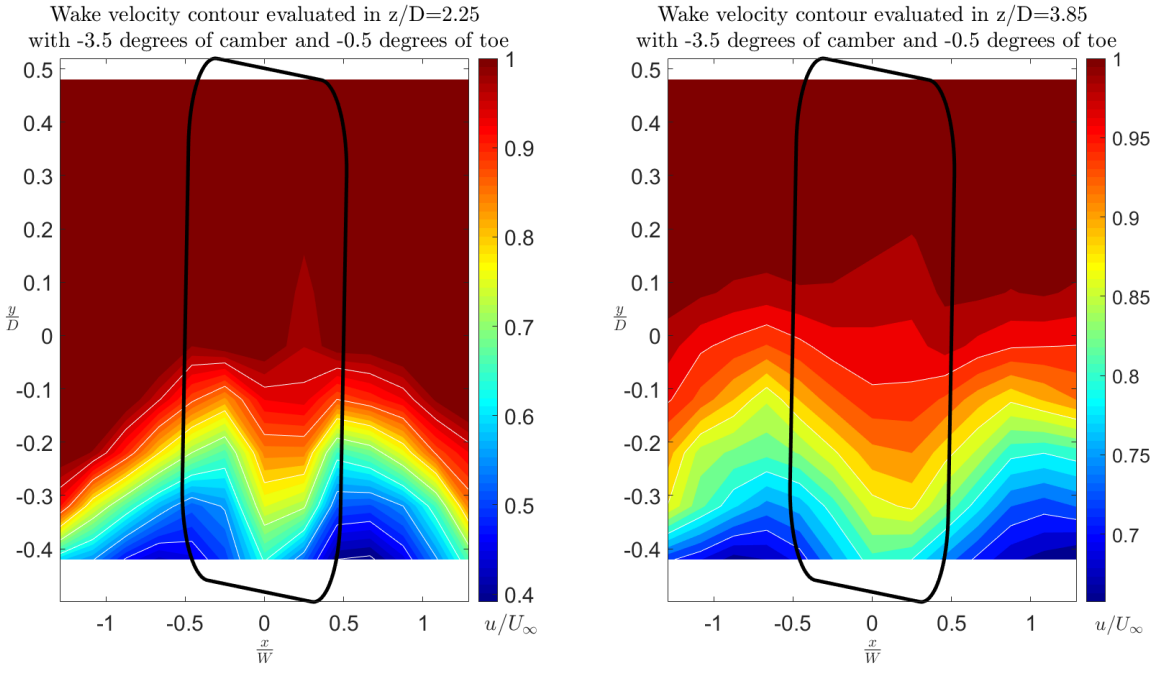

Figure 5.13: *Wake of rounded shoulder wheel with a camber angle equalo to -3.5° and a toe angle equalo to -0.5° at two different distances. On the left z/D=2.25 one the rigth z/D=3.85.*

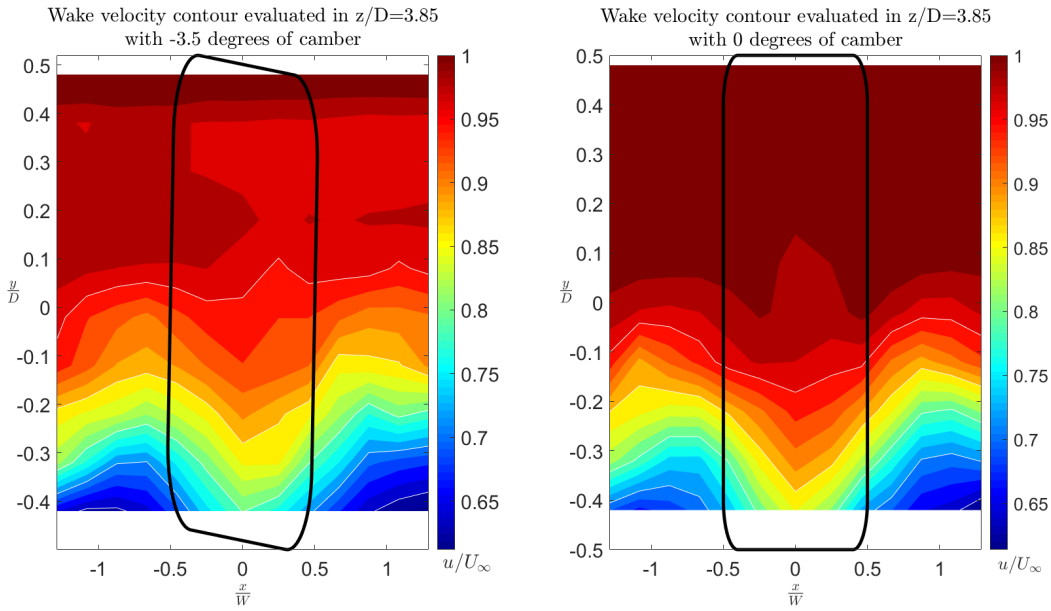

Figure 5.14: *Comparison of wake velocity contour between cambered and not cambered wheel in z/D=3.85. It can be seen a little asymmetry in the case of cambered wheel.*

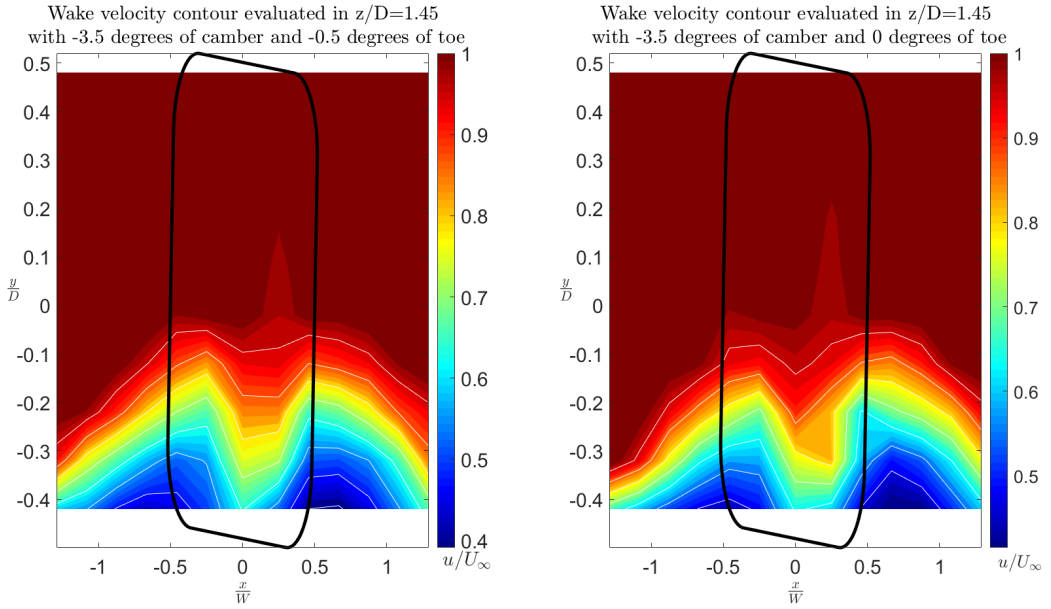

Figure 5.15: *Comparison of wake velocity contour between -0.5° of toe and 0° of toe in z/D=3.85. In this case the difference is very small. The wake profile in the case of a toe angle different from zero is larger on the left side rather than in the case of no toe angle.*

5.2.2 Extimation of the drag force

The resistance was evaluated through the implementation of the calculation of the energy contained inside the Trefftz plane, since the experiments were performed at a velocity too low to obtained a clear vale from the scale. The Trefftz plane is an immaginary plane perpendicular to the direction of the flow, in this plane it must be evaluated the integral over the surface of the kinetic energy. In order to do that it is necessary to be sufficeintly far from the body in exam in order to not over-estimate the drag. In this study it was obtained a drag coefficient of 0.98 obtained at a distance z/D=2.65. This is a reasonable value, compared with a standard value of drag coefficient equal to 0.95 for a wheel with the same aspect ratio in stationary conditions.[19]. The same study was performed for the 45-degrees shoulders wheel, obtaining an higher coefficient: Cd=1.3. Also the ratio between parallel and cambered wheel was estimated and an interesting result was obtained, the value of the ratio was very similar to the one of Saddington and Knowles [11]. In their experiments the ratio was equal to 0.8 while in this thesis it was obtained 0.82.

Wheel type	C_D
45° shoulders	1.3
Rounded shoulders	0.95
Parallel/Cambered	0.82 (ratio)

Table 5.1: *Resuming table of C_D in the case of rounded and 45 degrees shoulders, and ratio between parallel and cambered.*

5.2.3 Spectral analysis and comparison with CFD

Finally it was compared the velcoity contour of the wake of the rounded shoulder wheel with no angle of camber and toe with the numerical simulation obtained using adopting S-A equation. The simulations were performed with a rotating wheel in contact with the ground, with a Reynolds number equal to $1.34 \cdot 10^6$. The second comparison was made looking at the Strouhal number of DES model and the one obtaiend in this study. Some of the features present in the CFD velocity contour are also present in the experimental results. The enlargement of the wake, for instance, is felt in both cases. The shape in z/D=1.45 is very similar, in particular in the central region of the wake where two vertices are captured and between them, a region of higher velocity is present. Due to the encumbance of the hot wire it is not possibile to compare the results close to the ground. The velocity range is different between numerical and experimental results, this is due to the offset given by the pitot at low velocities. The spectral analysis was performed looking at the results obtained from the cylinder. In fact, the spectral analysis of the cylinder show that the highest peak occurs in a vertical coordinate equal to y/D=1 (where y/D=0 is at the cylinder center). The same was made in the wheel, to demonstarte that it was evaluated the spectrum in x/W=0 and changing the distance in y. The highest peak was reached in y/D=0.5 (the highest possible point aviable). The next step was to see how the spectrum changes in the spanwise direction. It can be seen that five prevalent peaks were captured by the spectral analysis. Also in the CFD simulation it was performed a spectral analysis, it was obtained by placing a 'fake' probe in the center of the wake at different distances. In that case the results were more evident as the distance increases from the wheel, in this study the spectral analysis was more accurate at the closest station. In the numerical simulation two main peaks were evaluated having two different Strouhal number: 0.17 and 0.34. In the experimental results 5 peaks were obtained:0.18,0.33,0.5,0.62 and 0.77. These five peaks can be attribuited to the different vortices that born in the different parts of the wheel.

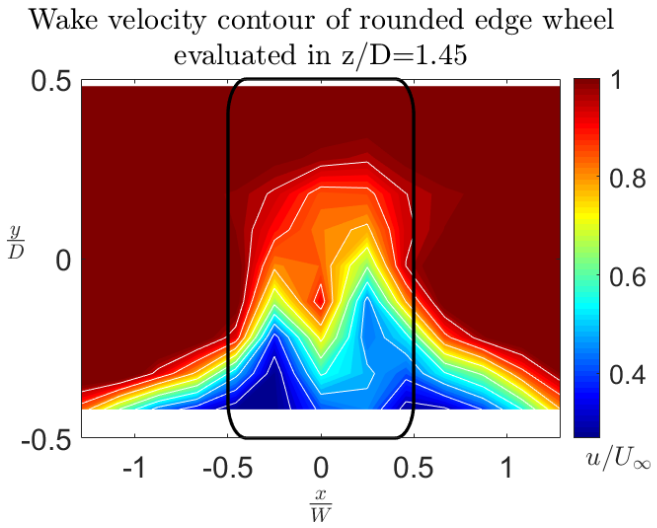

(a) *Experimental results*

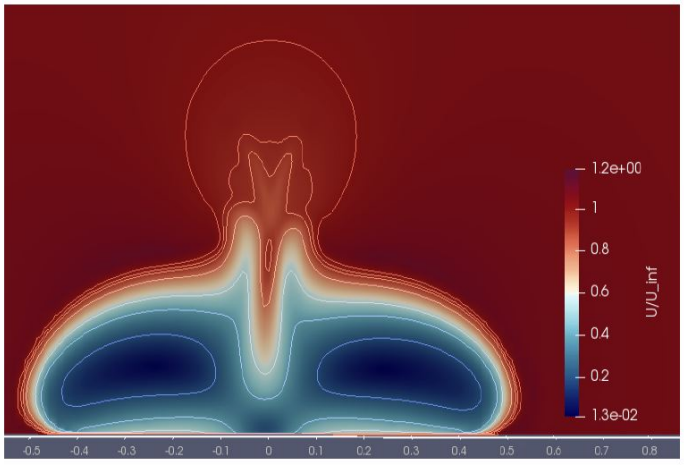

(b) *CFD results*

Figure 5.16: *Comparison of the results between experimental* (a) *and CFD* (b) *in z/D=1.45. Some similar features can be seen: the two symmetrical vertices located close to half wheel heigth;a region of faster velocity present at the lower center of the wheel; a circular region of lower velocity over the two vertices.*

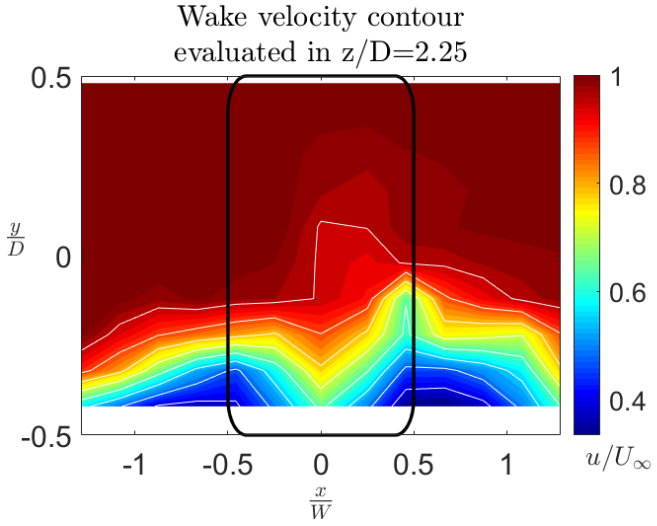

(a) *Experimental results*

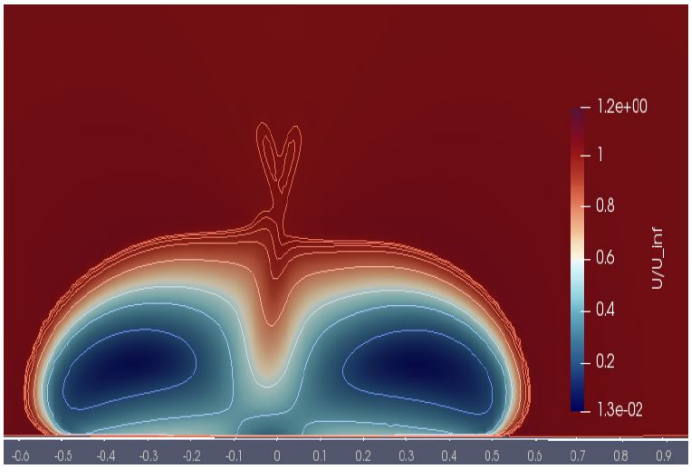

(b) *CFD results*

Figure 5.17: *Comparison of the results between experimental* (a) *and CFD* (b) *in z/D=2.25. In both cases there is no more the presence of the vertices, the wake is more relaxed and it starts to enlarge.*

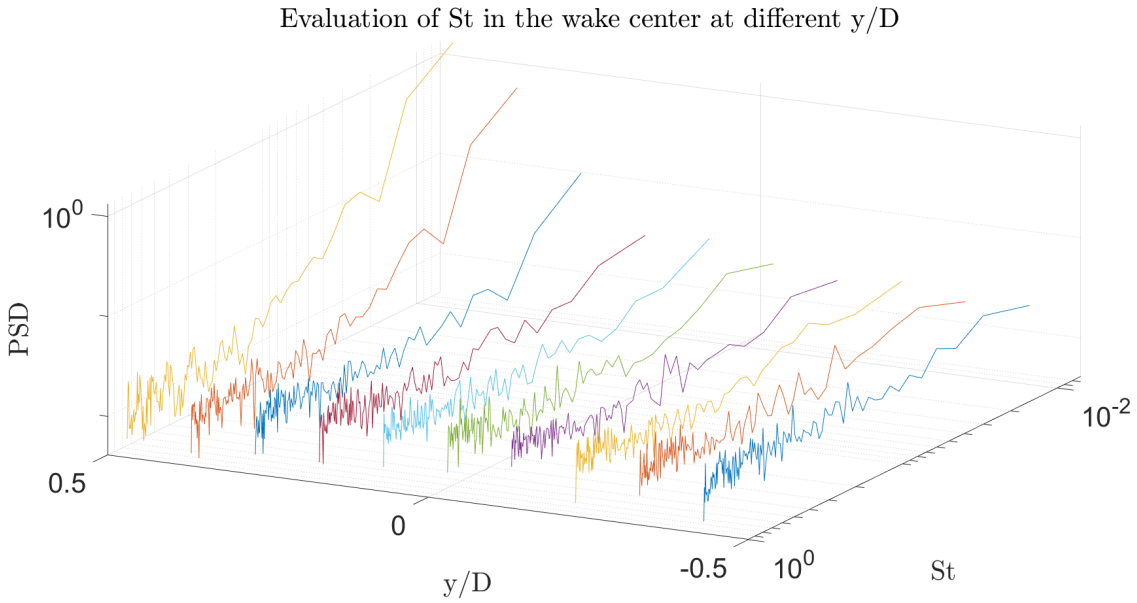

Figure 5.18: *Spectral analysis computed at wake center in different y/D. The location where the peaks are more relevant is in y/D=0.48, as y/D decreases the spectrum becomes flatter and more noisy.*

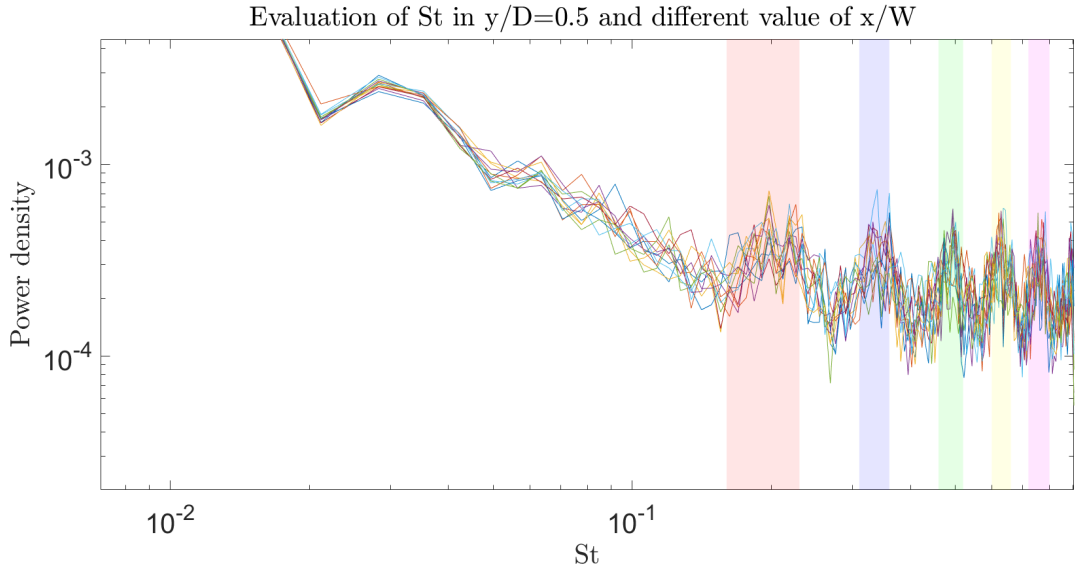

Figure 5.19: *Spectral analysis computed at y/D=0.5 at different values of x/W. It can be clearly seen the presence of five intervals of Strouhal number.*

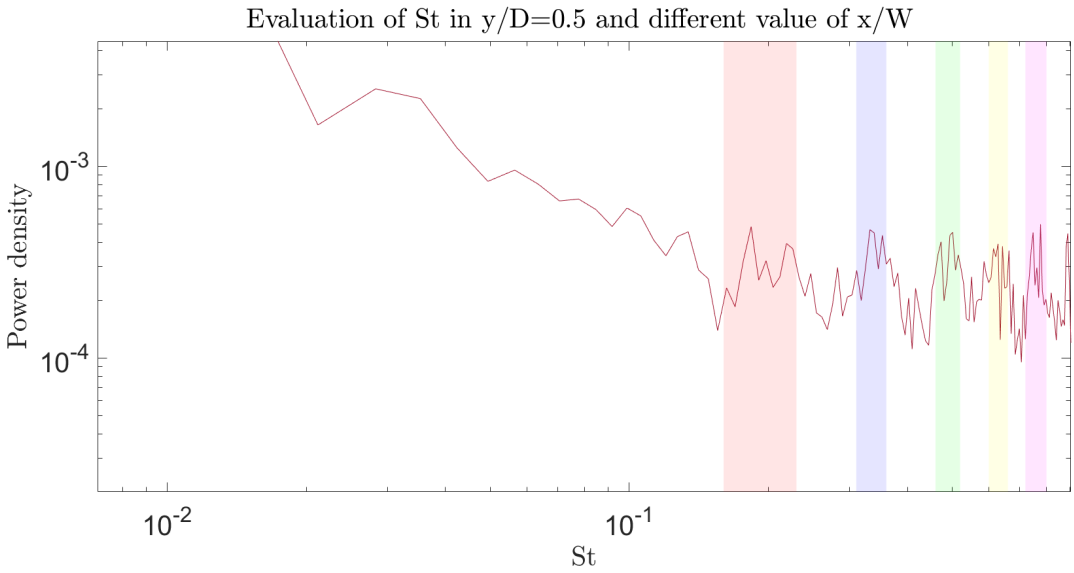

Figure 5.20: *Spectral analysis evaluated at y/D=0.5 and x/W=0. The peaks are inside the intervals previously reported and have similar results to the ones obtaiend ina CFD enviroment.*

Model	St
S-A	0.18;0.315
DES S-A	0.17;0.34
DDES S-A	0.2;0.335
Experiment	0.18;0.33;0.5;0.62;0.77

Table 5.2: *Comparison of Strouhal number evaluation between different type of modeling turbulence and experimental data.*

Chapter 6

Conclusions

Two main experiments have been conducted: the study of a cylinder and the study of different type of wheels. In the first case the mean wake profile was evaluated and the shedding frequency. As expected, it was found that the shedding frequency increases as the velocity increases, in particular the relation between the free stream velocity and the frequency is linear. From this relation it was obtained the Strohual number (St=0.19). It was also found that depending on the vertical position with respect the cylinder one or two harmonics can be seen, in particular if the sensor is inside the wake two harmonics are captured, while on the external region only one is seen. The last step of the study of the cylnder was the calibration of the hot-wire using the shedding frequency, obtaining results very similar to the one of the standard calibration (using the Pitot probe).

The study of the wheels was focused on geometrical parameters (shape of the shoulder, camber angle and toe angle) and the comparison of these results with the one of the CFD. For all the wheels it was evaluated the mean velocity profile of the wake. It was found that the wheel with sharp shoulders has a completely different wake with respect the other two wheels with a region of low velocity much larger, leading to have an higher resistance. In the case of rounded shoulders and 45° degrees shoulders two main vortices has been seen and the development of these vortices is very similar. An estimation of the drag was performed through the Trefftz plane, it was evaluated at z/D=2.65 and the drag coefficient obtained was equal to 0.98 for the case of rounded shoulders and 1.3 for the 45-degrees one. The rounded shoulders wheel was studied furthermore with a camber angle first (-3.5°) and a camber angle and a toe angle after (-3.5° and -0.5°). In the case of the camber angle it was seen the presence of a region of lower velocty much larger in the region where the wheel is more in contact with the ground. In the case of the toe and camber angle, no big differences were evaluated. In order to validate the numerical tecnhique used in the CFD, it were compared the velocity contour of the wake at two different distances from the rounded wheel. In the case of the CFD results, the wheel is in rotation, while in the case of this study the wheel is stationary. Also the Reynolds number is different, in the numerical computation the Reynolds number is equal to $1.34 \cdot 10^6$, in the experimantal case $Re = 8.2 \cdot 10^5$. Being an average quantity, it was compared with the S-A model. The results can be considered similar, most of the features of the wake were captured in both cases, for instance the changing of the shape with the increase of the distance, the presence of a region of higher velocity in the center of the wake in the closer station. Finally the spectral analysis was computed and compared with the one obtained throug the DES model. In the DES model two main peaks were found, related to two main frequencies. In the experimental results the peaks were five, in particular the first two with the same value of the numerical one.

This study can be considered the first step of a much bigger problem. In fact, this problem can be studied more accurately in different ways. First of all it can be interesting to make the wheels rotate and see how the wake changes.

This means to install a rotating belt in order to simulate the ground. Other geometrical parameters can be studied: the wheel hub and different type of hubs, different value of camber angles. Regarding the type of acquisition it can be interesting to acquire data with an X-wire, in order to capture two compoments of the velocity, it can be also interesnting to acquire simuntaneously the velcoity in two or more points of the wake in order to see the correlation of the shedding (in the case of the cylinder), or to make comparison with DES in different instants of time. Another aspect that can be studied is the interaction that generates the wake of the wheel with another body: another wheel or a wing profile. Last but not least it can be very usefull using a flow visualization method, for example the PIV technique in order to see istantaneously the profile of the wake in a much larger domain.

Acknowledgements

In primo luogo voglio ringraziare il Prof. Gabriele Bellani e l'Ing. Lorenzo Lazzarini che grazie alla loro disponibi lità e ai loro consigli mi hanno permesso di svolgere questa esperienza, facendomi appassionare ancora di più a questa materia. Voglio anche ringraziare tutti i tecnici presenti in hangar che mi hanno aiutato dal punto di vista pratico, realizzando componenti necessari per lo svolgere di questa tesi.

Ovviamente ringrazio la mia famiglia e mia nonna, senza i cui sacrifici non potrei essere qui. Grazie per essermi sempre stati vicino nei momenti più difficili e per avermi spronato ad andare avanti.

Ringrazio anche Cecilia, che mi ha sostenuto e creduto in me fin da subito, non le potrò mai essere grato abbastanza per quello che ha fatto.

Inoltre voglio ringraziare il coinquilino Marco, e i compagni di corso Davide, Giovanni, Federico, Gabriele che hanno reso questi anni indimenticabili. Ringrazio anche gli amici di Modena: Marco, Gianluca, Sara, Martina, Fabio e Andrea, loro sanno quanto ci tenga ad aver raggiunto questo obiettivo.

Bibliography

[1] Simulation Techniques for the Aerodynamic Study of Automotive Components, M. Pantalone, Univeristà di Bologna, 2018.

[2] Aerodynamic Design Considerations of a Formula 1 Racing Car. Ben Agathangelou and Mike Gascoyne. February 1998.

[3] Boundary layer theory. Dr Hermann Schlichting. McGraw Hill book company.

[4] Control of circular cylinder flow using distribuited passive jets. Ben L. Clapperton and Peter W. Bearman. Department of Aeronautics, Imperial collage, London, May 2018

[5] Bluff bodies aerodynamics. Lecture notes by Guido Buresti. Department of Aerospace Engineering University of Pisa, Italy. June 2000

[6] Vortex shedding from bluff bodies. G.Buresti. Chapter 4 in "Wind effects on buildings and structures" (Riera J.D A.G Eds) Rotterdam 1998.

[7] The vortex-shedding process behind two-dimensional bluff bodies By A. E. PERRY, M. S. CHONG AND T. T. LIM Department of Mechanical Engineering, University of Melbourne, Parkville, Victoria 3052, Australia

[8] A new Strouhal–Reynolds-number relationship for the circular cylinder in the range $47 < Re < 2 \cdot 10^5$. Uwe Fey, Michael König, and Helmut Eckelmann. July 1998.

[9] Flow visualization around a circular cylinder near to a plane wall. S. J. PRICE, D. SUMNER, J. G. SMITH, K. LEONG AND M. P. PAIGDOUSSIS. Department of Mechanical Engineering, McGill University Montreal, QueHbec, Canada. 2001.

[10] The Aerodynamics of an Isolated Wheel Rotating in Contact with the ground by John Edward Fackrell. 1974.

[11] On the Near Wake of Rotating, 40% Scale Champ Car Wheels. Robin Knowles, Alistair Saddington and Kevin Knowles. 2002

[12] A guided tour of the fast Fourier transform. G. D. Bergland. 1969.

[13] The Use of Fast Fourier Transform for the Estimation of Power Spectra: A Method Based on Time Averaging Over Short, Modified Periodograms. PETER D. WELCH. 1967.

[14] What does the hot-wire measure? By Fredrik Laurantzon, Nils Tillmark and P. Henrik Alfredsson. CCGEx, KTH Mechanics, SE-100 44 Stockholm, Sweden Technical Report

[15] Pitot probe corrections in fully developed turbulent pipe flow. B.J.McKeon, J.Li, W.Jiang, J.F.Morrison and A.J.Smits

[16] Hot wire anemometry, Lecture notes by Alessandro Talamelli and Gabriele Bellani.

[17] Time-frequency analysis and its applications - Hilbert transform and applications, G.Buresti.

[18] Experimental and numerical studies of the flow over a circular cylinder at Reynolds number 3900. Philippe Parnaudeau, Johan Carlier, Dominique Heitz, and Eric Lamballais. 2008.

[19] Race car aerodynamics by Joseph Katz